Norwegian University
of Life Sciences

Master's Thesis 2017 60 ECTS
Faculty of Chemistry, Biotechnology and Food Science

Roles of Charged Residues in the Active Site of Lytic Polysaccharide Monooxygenase – Effect on Catalysis

Victoria Karlsen
Master of Chemistry

ACKNOWLEDGEMENTS

The work presented in this thesis was carried out in Morten Sørlie's (Bioorganic) research group and the Protein Engineering and Proteomics (PEP) group at the Faculty of Chemistry, Biotechnology and Food Science at the Norwegian University of Life Sciences (NMBU) in the period from June 2016 to May 2017. This thesis was part of a larger research project where the objective was to unravel the molecular basis of LPMO activity.

First and foremost, I would like to express my gratitude to my supervisor Professor Morten Sørlie for offering me to work in his research group. I really appreciate all your help, support and encouragement that have helped me to from when I embarked in this new and exciting research field to submitting the master thesis. I would also like to express my gratefulness to my co-supervisors Dr. Anne Grethe Hamre, Dr. Åsmund Kjendseth Røhr and Dr. Bastien Bissaro for your practical advises in the lab. Thank you for being so patient, and for always sharing your valuable time with me.

Thanks to my fellow students Daniel Gustavsen, Julie Strømberg, Lars-Inge Gammelsæter Johnsen, Anders Haukebø, Alexander M. Wathne, Sara Johanne, Rim Al-Sadawi and Helene Bjølgerud for the fun lunch breaks and all your support throughout the year. I want to give special thanks to Sunniva Tangen Haldorsen, Marta Sofie Norheim Tvetene and Sondre Norheim Tvetene for all the fun evenings with board games, watching movies, and other social events. The year would have been dull and gray without you all!

Finally, special thanks to my family for believing in me and giving me the determination to strive towards my goals and to fulfill this five-year long education. Words cannot express how grateful I am to my parents, Sissel-Anne Karlsen and Arild Oskar Karlsen, and my sister Therese Karlsen, which have helped and supported me to get to where I am today.

Victoria Karlsen
Ås, May 2017

SUMMARY

Lytic Polysaccharide monooxygenases (LPMOs) are copper-dependent enzymes that catalyze the oxidative cleavage of glycosidic bonds in polysaccharides in the presence of H_2O_2 or molecular oxygen paired with a reductant. LPMOs have an essential role in biomass saccharification in biorefineries, as they break down the recalcitrant crystalline substrates such as cellulose and chitin, which enable glycoside hydrolases to depolymerize the substrate into glucose units. This thesis was written as part of a larger research project where the objective was to acquire knowledge of the molecular mechanism of LPMO activity. The work in this thesis provides site-directed mutagenesis data for probing the roles of glutamate (Glu217) and arginine (Arg212) in the active site of the cellulose-active CelS2 (PDB id: 4OY7), which will provide as basis for further studies to unveil the molecular basis in their catalysis.

CelS2 differ from other cellulose-active LPMOs in terms of the active site architecture, with the amino acids glutamate (Glu217), arginine (Arg212) and phenylalanine (Phe219) that lies in close proximity to the copper ion in the active site. First, Glu217 was mutated into glutamine (Glu217Gln) to resemble other cellulose-active LPMOs, and the results showed that the mutant Glu217Gln functioned as well as the wild-type. Furthermore, Glu217 was mutated into aspartate and asparagine to position the polar group from the copper ion, which proved to be detrimental for CelS2 activity. Finally, CelS2-Glu217Ala was made to remove the carboxylate group completely that also abolished the activity, which is in consensus to previous studies with *Tt*LPMO9-Q151L (Harris et al., 2010) and CBP21-E60A (Loose et al., 2016b) mutants. Altogether, these data indicate that glutamate in CelS2 and glutamine in other cellulose-active LPMOs are essential for LPMO activity and have the same role in catalysis, most likely to coordinate the co-substrate towards the copper ion for the formation of superoxide that is used for oxidative cleavage of polysaccharides.

Arginine was mutated into lysine (Arg212Lys) to eliminate the guanidinium group of arginine, which is postulated to contribute a stabilizing effect under catalysis. However, Arg212Lys made no difference to CelS2 activity. Thus, more fundamental work is required to understand the roles of amino acids involved in LPMO activity.

SAMMENDRAG

Lytisk Polysakkarid Monooksygenaser (LPMOer) er kopper-avhengige enzymer som katalyserer oksidativ spaltning av glykosid bindinger hos polysakkarider med bruk av H_2O_2 eller molekylær oksygen sammen med en reduktant. LPMOer har en svært viktig rolle i biomasse sakkarifisering i bioraffinerier, ettersom de bryter ned trassig krystallinsk cellulose og kitin som gir glykosid hydrolaser muligheten til å depolymerisere substratet ned til glukose enheter. Denne masteroppgaven er del av et større forskningsprosjekt der målet er å tilegne seg kunnskap om det molekylære mekanismen for LPMO aktivitet. Arbeidet presentert i denne masteroppgaven tilbyr site-directed mutagenesis data for tolkningen av rollen til glutamat (E217) og arginin (R212) i det aktive setet hos den cellulose-aktive CelS2 (PDB id: 4OY7), som vil fungere som et grunnlag for videre studier på å avdekke det molekylære grunnlaget for deres katalyse.

CelS2 skiller seg fra andre cellulose-aktive LPMOer med tanke på arkitekturen på det aktive setet, med sine aminosyrer glutamat (E217), arginin (R212) og fenylalanin (F219) som ligger nært kopper ionet i det aktive setet. Først, ble E217 mutert til glutamin (E217Q) for å ligne på de andre cellulose-aktive LPMOer, og resultatet var at mutantet viste seg å fungere like effektiv som vill-typen. Videre ble E217 mutert til aspartat og asparagin for å flytte den polare gruppen vekk fra kopper ionet, noe som resulterte i fullstendig tap av CelS2 aktivitet. Tilslutt, ble CelS2-E217A mutanten laget for å fjerne karboksylat gruppen som også førte til fullstendig tap av aktivitet, som er i overenstemmelse med tidligere studier med *Tt*LPMO9-Q151L (Harris et al., 2010) og CBP21-E60A (Loose et al., 2016b). Tilsammen, tyder disse dataene på at glutamat hos CelS2 og glutamin hos de andre cellulose-aktive LPMOer er essensielt for LPMO aktiviteten og har den samme rollen under katalysen, mest sannsynlig koordinerer de ko-substratet nærmere mot kopper ionet for å danne superoksidet som er ansvarlig for det oksidative spaltningen hos polysakkarider.

Arginin ble mutert til lysin (R212K) for å eliminere guanidinium gruppen til arginin, fordi vi tror den bidrar med en stabilisere effekt under katalysen. Dessverre, viste mutanten ingen effekt på CelS2 aktiviteten. Derfor, trengs mer grunnleggende arbeid for å oppnå en forståelse for rollen til aminosyrer involvert i LPMO aktiviteten.

TABLE OF CONTENTS

ABBREVIATIONS

AA	Auxiliary activity
Ala (A)	Alanine
Ao	*Aspergillus oryzae*
Arg (R)	Arginine
Asp (D)	Aspartic acid / aspartate
Aspartate	Deprotonated aspartic acid
Asn (N)	Asparagine
CAZy	Carbohydrate-active enzymes
CBH	Cellobiohydrolase
CBM	Carbohydrate-binding module
CBP	Chitin-binding protein
CDH	Cellobiose dehydrogenase
Cj	*Cellvibrio japonicus*
$_{D}$-GLC	Dextrorotatory (+) glucose
EG	Endoglucanase
EPR	Electron Paramagnetic Resonance
ET	Electron transfer
Ef	*Enterococcus faecalis*
ExPASy	Expert Protein Analysis System
GH	Glycoside hydrolase
GlcGlc1A	(C1)-Oxidized cello-oligosaccharide with a degree of polymerization of 2
$(Glc)_2Glc1A$	(C1)-Oxidized cello-oligosaccharide with a degree of polymerization of 3
Glu (E)	Glutamic acid / glutamate
Glutamate	Deprotonated glutamic acid
Gln (Q)	Glutamine
His (H)	Histidine
HPAEC	High Performance Anion Exchange Chromatography
ICS	Ion Chromatography System
IEC	Ion Exchange Chromatography
ITC	Isothermal Titration Calorimetry
LB	Luria-Bertani

LDS	Litium Docedyl Sulphate
Lm	*Listeria monocytogenes*
LP	Low Pressure
LPMO	Lytic Polysaccharide Monooxygenase
Lys (K)	Lysine
MES	2-(*N*-morpholino)ethanesulfonic acid
Mt	*Myriococcum thermophilum*
Nc	*Neurospora crassa*
NMR	Nuclear magnetic resonance
Phe (F)	Phenylalanine
PyMOL	molecular visualization program of protein crystals
PAD	Pulsed Amperometric Detection
Sm	*Serratia marcescens*
SEC	Size Exclusion Chromatography
SOC	Super Optimal Broth
SOD	Superoxide Dismutase
Ta	*Thermoascus aurantiacus*
Tyr (Y)	Tyrosine
WT	Wild-type

1. INTRODUCTION

Petroleum have given the modern society many advantages such as economic growth, mobility of labor force and reduced energy poverty. Two-third of the fossil fuel is used to power the transportation sector, while the remaining one third is applied in agriculture, fisheries, constructing industries, pharmacies, cosmetics, feed, and battery (Wyman et al., 2005). The golden age with petroleum is facing an end as the natural, limited reservoir is slowly emptying. In this respect, plant carbohydrates present an opportunity to improve energy security, as this resource represents an abundant and renewable source of carbon. With the use of plant carbohydrates follows new challenges that need to be addressed. Carbohydrates such as cellulose in woods are recalcitrant materials to degrade, as they are insoluble and highly crystalline. A promising approach for overcoming recalcitrance is a two-step treatment; first, cellulose is treated with harsh chemicals to disrupt the crystalline structure (termed pretreatment), and then treated by cellulose-active enzymes that depolymerize cellulose into glucose units (saccharification). Glucose can be fermented into bioethanol or used as building blocks for production of plastic, textile, emulsion-stabilizer in food, and much more. As bioethanol is competing in price with fossil fuel, gas and coal, the key solution to commercialize second-generation fuel from wood is to reduce processing costs and improve the tools of biotechnology (Wyman et al., 2005).

In Nature, fungi play the pivotal role for degrading biomass and recycling carbon on Earth. Fungi, actinomycete bacteria and most other biomass-degrading organism secrete complex enzyme cocktails, whereas the primary component is glycoside hydrolases (GHs). GHs are responsible for hydrolysis of glycosidic bonds between two carbohydrate moieties, and thus are the main driving force for degrading carbohydrates. They are accompanied by glycosyl transferases, polysaccharide lyases, carbohydrate esterases and non-catalytic carbohydrate-binding modules, which contribute to saccharification in different ways (Payne et al., 2015). Such enzymes provide a good starting point for researchers to design industrial enzyme cocktails. Recently, a new key class of enzymes was discovered that was capable of enhancing depolymerization of recalcitrant cellulose significantly (Vaaje-Kolstad et al., 2010; Harris et al., 2010). In contrast to the hydrolyzing properties of GHs, these new enzymes perform oxidative cleavage on the crystalline region of cellulose with the use of molecular oxygen, and thus were termed lytic polysaccharide monooxygenases (LPMOs).

In this introduction, after dealing with the inert nature and complexity of cellulose (see section 1.1), we will focus on the newly discovered lytic polysaccharide monooxygenases in terms of protein structure and molecular basis of activity.

1.1. CELLULOSE

Plant carbohydrates primarily consist of cellulose, the linear unbranched homopolymer of β-$_D$-glucopyranose units linked by (1 - 4)-glycosidic bonds (O'Sullivan, 1997), where each unit is rotated 180° according to adjacent unit, making the disaccharide cellobiose the repeating unit (**Fig. 1.1.1**). Interestingly, a cellulose chain can be as long as 10 000 units in Nature (O'Sullivan, 1997). Furthermore, the pyran rings exist most commonly in chair conformation, meaning that the hydrogens lie in axial position and hydroxyls in equatorial. Thus, adjacent cellulose chains can bind together by hydroxyls via a hydrogen-bonding network, resulting a sheet (¨layer¨) planar to the pyran rings (**Fig. 1.1.1**). The formation of sheets usually happens when cello-oligosaccharides are longer than DP8 (degree of polymerization), as the affinity to another cellulose chain is larger than to the aqueous solvent (Brown, 2004). Notably, hydrogen lie perpendicular to the plane of the sheet, giving a hydrophobic face both over and under the sheet, which enables other cellulose sheets to pack together by several van der Waals interactions and inter-sheets hydrogen bonds, forming the microfibril (**Fig. 1.1.2**). The hydrophobic surface of the microfibril is usually coated by a dense layer of water (hydrophobic hydration), which makes crystalline cellulose highly resistant to acidic hydrolysis (Himmel et al., 2007).

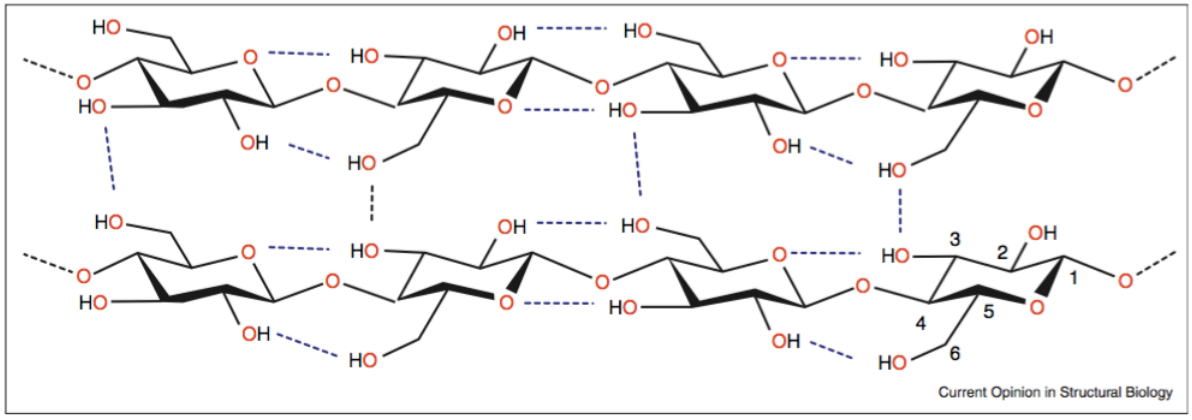

Figure 1.1.1. Cellulose structure, showing the intra-sheet network of hydrogen bonds. The distance between two pyran rings on the adjacent cellulose chains is 8.2 Å, while the distance between of C1 from one ring and C1 to the next on the same cellulose chain is 5.2 Å. Figure taken from Hemsworth et al., 2013.

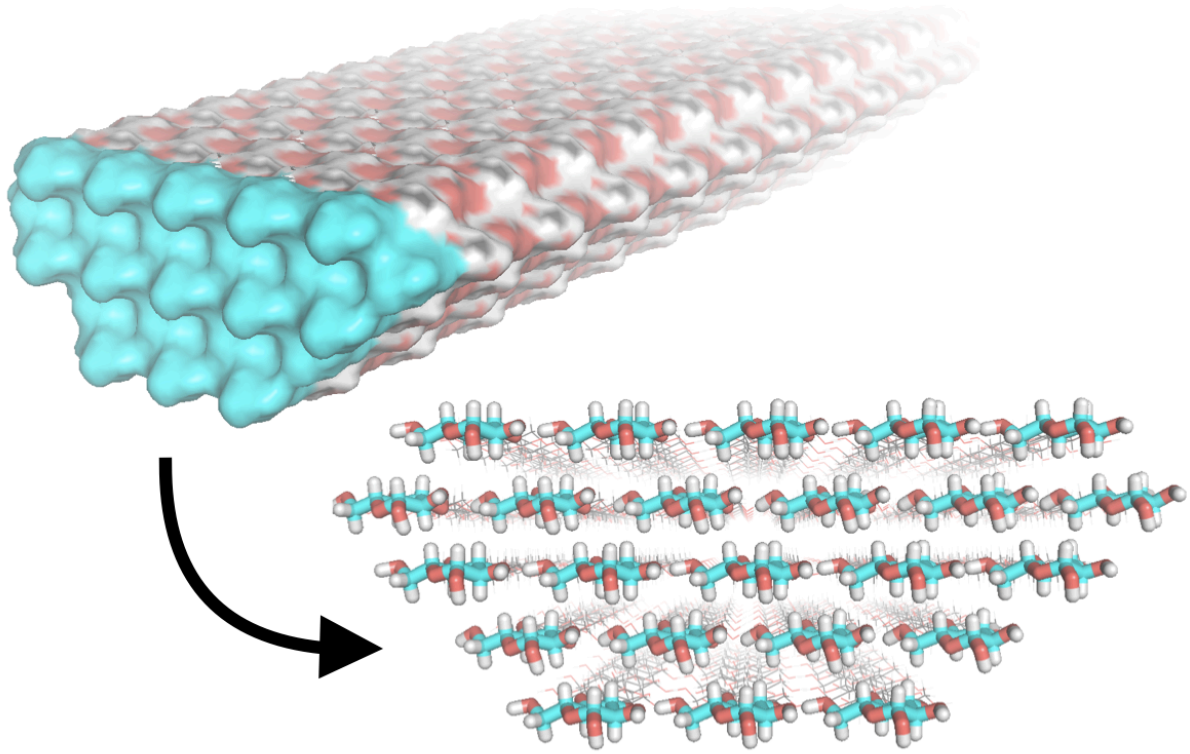

Figure 1.1.2. Microfibril. An overview of the microfibril to the left, and the fiber end is viewed to the right. Monomers shown in blue indicate the first $_D$-GLC monomers in each chain. This cellulose fiber consists of five sheets, whereas adjacent chains on a plane is linked by hydrogen bonding to form one sheet (¨layer¨ of the microfibril). Several sheets, arranged on top of each other, form one microfiber.

In Nature, the microfibrils can exist as one or several crystalline structures (polymorphism), such as the allomorphs cellulose Iα and Iβ (O'Sullivan, 1997) (**Fig. 1.1.3**). The primary difference between these two lies in the hydrogen bonding patterns (Payne et al., 2015). Iα allomorph has a triclinic unit cell, while Iβ has a monoclinic unit cell that is formed by two chains named origin and center (Poma et al., 2016). Notably, the allomorph Iβ (D = 3.89 Å) is packed denser than Iα (D = 3.91 Å), making Iβ more thermodynamically stable. Cellulose Iβ can be found in great quantity in cell-wall of higher plants, such as cotton, wood and ramie, whereas greenalgae and *Valonia* (¨bubble algae¨) are rich with cellulose Iα (Payne et al., 2015). Interestingly, some bacteria are capable of synthesizing cellulose Iα used to form a protective envelope around the cells (Ross et al., 1991).

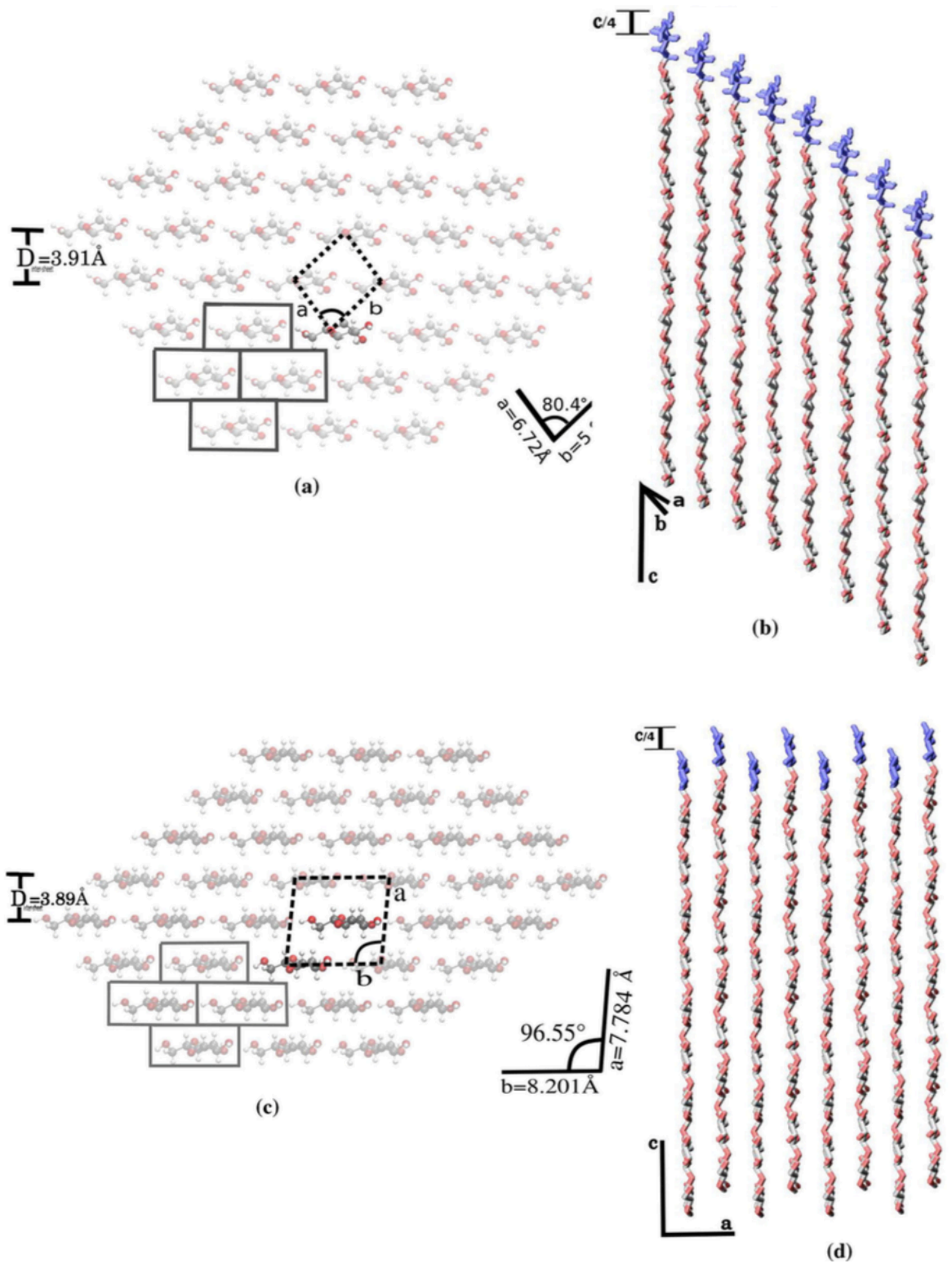

Figure 1.1.3. Cellulose Iα versus Iβ. (a) Iα allomorph, viewed from the microfiber end. Axes a and b define the triclinic unit cell formed by one chain. **(b)** Display the layer packing in cellulose Iα. Monomers shown in blue indicate the first $_D$-GLC monomers in each layer. **c, d** are similar to **a, b** respectively but they illustrate the structure of Iβ. Figure taken from Poma et al., 2016.

1.1.1 PRETREATING LIGNOCELLULOSIC BIOMASS

In Nature, cellulose is mostly found in plant cell-walls companied with hemicellulose and lignin, as well as minor fractions of pectin, glycoproteins, lipids, minerals, and soluble sugars (Sjöström, 1993) (**Fig. 1.1.4**). Hemicellulose integrates the cell-wall structure by cross-linking to several cellulose fibers and other constituents, yielding the complex composite structure found in plants and trees. Together with lignin, a high molecular phenolic heteropolymer, provide mechanical support and strength to the cell-walls (Payne et al., 2015). The ratio of cellulose, hemicellulose and lignin differs greatly between plant species. For example, hard- and softwood are generally rich in cellulose and lignin, which favors rigidity, whereas agricultural plants have a relative high content of hemicellulose, making their tissue more flexible than wood (Olsson et al., 2004). The complex and heterogeneous nature of biomass limits the transport of enzymes to their substrate (Himmel et al., 2007).

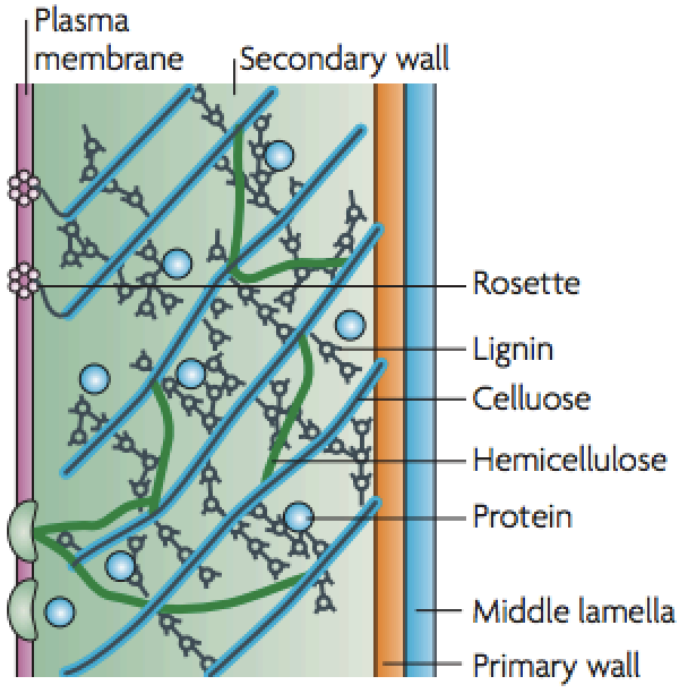

Figure 1.1.4. Cell-wall structure. Plant cell-wall consists mainly of cellulose (blue), hemicellulose (green) and lignin (black rings). Figure taken from Sticklen, 2008.

An effective pretreatment disrupt the cell-wall matrix that enables enzymes to penetrate the matrix and reach the target substrate (Igarashi et al., 2007). Pretreatment may in some degree disrupt crystalline cellulose into amorphous regions (i.e. lower degree of order), especially on the microfibril ends and the solvent-exposed cellulose chains on the microfiber surface (O'Sullivan, 1997). Most pretreatment methods retain the native cellulose allomorph, although certain treatment, e.g. with ionic liquids such as concentrated sodium hydroxide that swells the native fiber resulting a rearrangement of the cellulose chains, forming a new allomorph termed cellulose II (O'Sullivan, 1997). In contrast to native cellulose, the sheets of cellulose II lie in an antiparallel arrangement and exhibit a three-dimensional hydrogen-bonding network (**Fig. 1.1.5**). If cellulose II or native cellulose is treated further with liquid ammonia or some amines, forms cellulose III_{II} and III_{I} respectively (O'Sullivan, 1997). Cellulose III has shown to have significantly lower recalcitrance to enzyme deconstruction than native cellulose I (Igarashi et al., 2007; Beckham et al., 2011). Additionally, some studies have postulated the existence of cellulose IV, however, other studies indicate otherwise as they point out that this allomorph was cellulose Iβ all along (Nishiyama et al., 2009; Thomas et al., 2013; Wada et al., 2004). Altogether, pretreatment can reduce the recalcitrance that limits enzymatic hydrolysis, by removing cell-wall constituents such as lignin and hemicellulose, which function as a protective barrier to cellulose, and disrupt the crystalline cellulose into a more amorphous character.

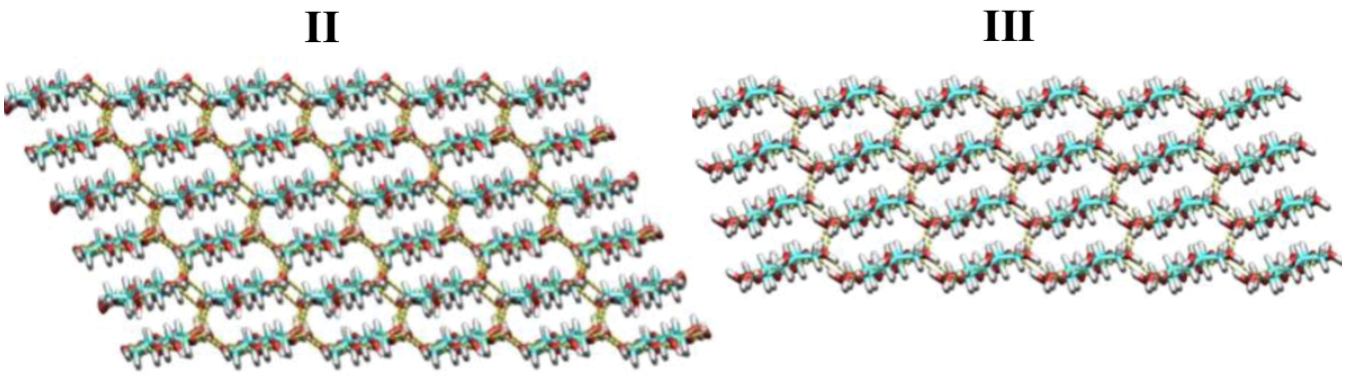

Figure 1.1.5. Synthetic cellulose allomorphs. The microfibril end for each of the two allomorphs is shown, depicting the three-dimensional hydrogen-binding network. Figure taken from Payne et al., 2015.

1.1.2. ENZYMATIC HYDROLYSIS OF LIGNOCELLULOSE

Three types of glycoside hydrolases are necessary for complete hydrolysis; (1) exoglucanases (also termed cellobiohydrolases (CBH)) attack chain ends and release cellobiose units, (2) endoglucanases (EG) that randomly cleave chains internally and creates new chain ends that CBH can depolymerize, and (3) β-glucosidases hydrolyze cellobiose into monomeric glucose, mitigating CBH product inhibition arising from cellobiose (Henrissat, 1985). These enzymes work in synergy as they enhance the activity of each other, and contribute to an efficient degradation of lignocellulosic biomass.

An enzyme cocktail with these three main catalytic activities is not enough to achieve the maximum theoretical yield of glucose per kilo lignocellulosic biomass (Harris et al., 2010). Some degree of crystalline cellulose remains even after pretreatment and enzymatic hydrolysis. Both cellobiohydrolases and endoglucanases struggle to perform hydrolysis on crystalline cellulose. Catalysis of CBH involves breaking several intralayer hydrogen bonds (require between 5.4 and 6.7 kcal/mol) to thread the chain into the active site for hydrolysis (**Fig 1.1.1** and **Fig 1.1.6**) (Beckham et al., 2011). Depolymerization of solubilized chains is much easier (3.4 kcal/mol) in comparison to crystalline cellulose, which has a rigid hydrogen-bonding network that contribute to recalcitrance. Thus, crystalline cellulose require strong binding to the chain end for CBH to manage several hydrolysis before dissociating from the substrate (¨exhaustion¨), however, the strong binding reduces the rate of depolymerization. The hydrolytic catalysis of endoglucanases requires a transition of conformation to the glucose ring from chair- to the unfavorable half-chair- or boat-conformation, which most likely is prevented by the strong hydrogen-bonding network (Rye & Withers, 2000). Thus, neither cellobiohydrolases nor endoglucanases are specialized in degrading the crystalline character of cellulose. Thus, the enzyme cocktail with only glycoside hydrolases is too inefficient and expensive to make biorefineries profitable, due to the slow kinetics of crystalline cellulose degradation (Hemsworth et al., 2016). This is where LPMOs comes in handy.

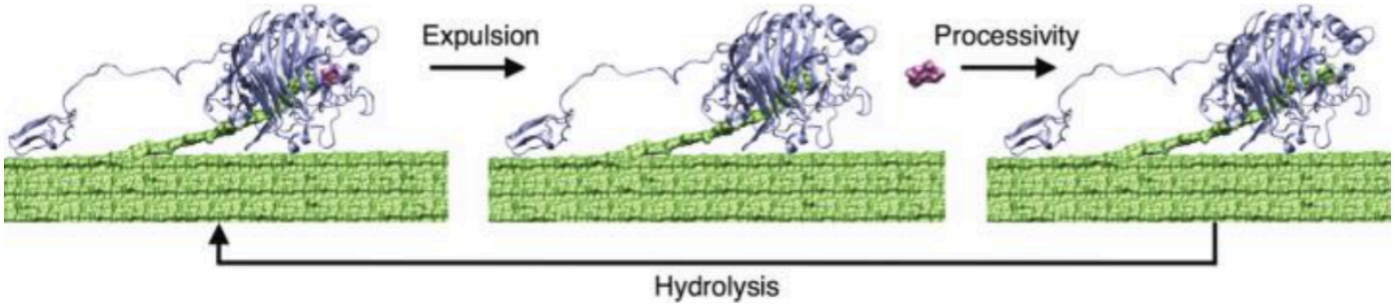

Figure 1.1.6. Catalytic cycle of a processive cellobiohydrolases (CBH). CBH (purple) thread the cellulose chain (green) into its active site for hydrolysis. From left to right; (1) CBH perform hydrolysis, (2) release of product (cellobiose, shown in pink), and (3) threading (or processivity or progression) of another disaccharide unit into the active site for further catalysis. Figure taken from Beckham et al., 2011.

Lytic polysaccharide monooxygenases attack crystalline cellulose by performing oxidation on the carbons adjacent to the glycosidic bond, resulting a highly unfavorable state that lead to a spontaneous breakage of the glycosidic bond. Thus, leaving a permanent mark on the cellulose chain, which prevents reforming the glycosidic bond and, in some degree, reprecipitation. The activity of LPMO have demonstrated a significant increase of glucose yield by two-fold, as cellobiohydrolases get access to new solubilized chain ends in crystalline context (Harris et al., 2010). These essential improvements in carbohydrate degradation have placed LPMOs at the center of worldwide research conducted on biomass conversion, and great efforts are made to unravel the molecular basis for their activity.

1.2. LYTIC POLYSACCHARIDE MONOOXYGENASE

The first lytic polysaccharide monooxygenases (LPMOs), not known to be oxidative enzymes at that time, were identified in the early 1990s. These enzymes were originally reported to be chitin-specific carbohydrate binding modules (CBM33) or sluggish glycoside hydrolases (GH61) (Schnellmann et al., 1994; Raguz et al., 1992; Armesilla et al., 1994). This *a posteriori* misclassification and the fact that the former are mainly of bacterial origin while the latter are essentially expressed by fungi contributed to the development of unrelated, parallel researches on both enzyme classes for nearly two decades after initial discovery. In the late 2000s, GH61 enzymes, which were known to lack measurable endoglucanase activity, showed a significant boosted activity with the presence of divalent metal ions (Harris et al., 2010). This discovery was led by the fact that the presence of divalent metal ions was mandatory for successful crystallization of these enzymes in NMR (Karkehabadi et al., 2008). Finally, the relevant pieces were put together by Vaaje-Kolstad *et al.* (2010), who discovered that these enzymes introduce chain breaks in crystalline polysaccharides with the use of molecular oxygen and a reductant. Accordingly, GH61s and CBM33 were then reclassified as auxiliary activity enzymes (AAs) (Horn et al., 2012).

1.2.1 AUXILIARY ACTIVITIES

As the LPMOs were unraveled, the enzymes belonging to GH61 and CBM33 were reclassified to auxiliary activities (AA) family 9 and 10 respectively, together with two newly discovered families in AA11 (Hemsworth et al., 2014) and AA13 (Vu et al., 2014; Leggio, 2015) in the Carbohydrate Active enzyme (CAZy) database. The CAZy database (cazy.org) was founded in 1991 by Bernard Henrissat and covers an overview of the different families of CAZymes. Currently one can find 27 enzymes in AA9 (10 of those is structurally characterized); 19 in AA10 (15 structures); one in AA11; and 3 characterized in AA13 (one structure). These families are categorized based on sequence similarities (Levasseur et al., 2013). AA9 and AA11 enzymes are exclusively fungal in origin, active on cellulose (Quinlan, et al., 2011; Phillips et al., 2011), oligosaccharides (Isaksen, 2014), hemicelluloses (Agger et al., 2014), xylan (Frommhagen et al., 2015), and chitin-activity of AA11 (Hemsworth et al., 2014). AA10 LPMOs are mainly found in bacterial genomes (with some viral members), and are active on chitin and cellulose (Forsberg et al., 2014). AA13 are fungal LPMOs that are active on starch derivatives, the only currently known LPMO substrates with α-linkages (Leggio et al., 2015; Vu et al., 2014). According to the known

structures of the different LPMOs, they all share a high degree of structural similarity (Vaaje-Kolstad et al., 2017).

1.2.2. GLOBAL STRUCTURE

The crystal structures revealed a compact β-sandwich core structure consisting of two β-sheets comprising seven or eight β-strands in total (**Fig. 1.2.1**). This structure is rigid due to two disulfide bridges that contribute to structural stability, Cys-39 and Cys-169 in the helical-strand region and between Cys139 and the C-terminal amino acid, Cys227 (*Nc*LPMO9C numbering). The former disulfide bridges, which connects loop L2 to strand β8, is common in all known LPMO9 structures, while the latter disulfide bridge is observed in about half of LPMO9s with known structures (Borisova et al., 2015). Most of the structural diversity lies in the series of short loops located between β-strands, whereas longer loops often contain short helices that build the flat surface for binding to carbohydrates. Loop between the first and third β-strand (second for fungal LPMOs) is called ¨loop 2¨ (abbreviated ¨L2¨). On the opposite side of the pyramide-like structure, lies region LS (loop short) and LC (long C-terminal loop) (Beeson et al., 2015; Wu et al., 2013). Some LPMO9s show a characteristic insertion between b-strands 3 and 4, called L3, which interacts with the L2 loop (Borisova et al., 2015). These loops vary greatly among LPMOs, and are thought to function in substrate recognition and specificity as they constitute large parts of the substrate-binding surface. In the middle of the flat substrate-binding surface lies the active site that catalyzes oxidative cleavage of carbohydrates.

The active site lies on the surface of the flat binding site and reveals a tightly bound copper ion coordinated by three nitrogen ligands contributed by two histidine residues, of which one is N-terminal, in a motif termed the histidine brace (Quinlan et al., 2011; Aachmann et al., 2012), see section 1.2.7 for further details. The first crystal structures of LPMO did not reveal the native metal to LPMOs as they were bound to many different divalent metal ions (Vaaje-Kolstad et al., 2005; Karkehabadi et al., 2008). According to the binding studies with isothermal titration calorimetry (ITC) done by Quinlan et al. (2011), the LPMOs bounded poorly to divalent metal ions such as Mg^{2+}, Ni^{2+} and Zn^{2+}, but bounded strongly to Cu^{2+} ion with a clear 1:1 metal:LPMO stoichiometry. Thus, LPMOs were characterized as copper-dependent enzymes.

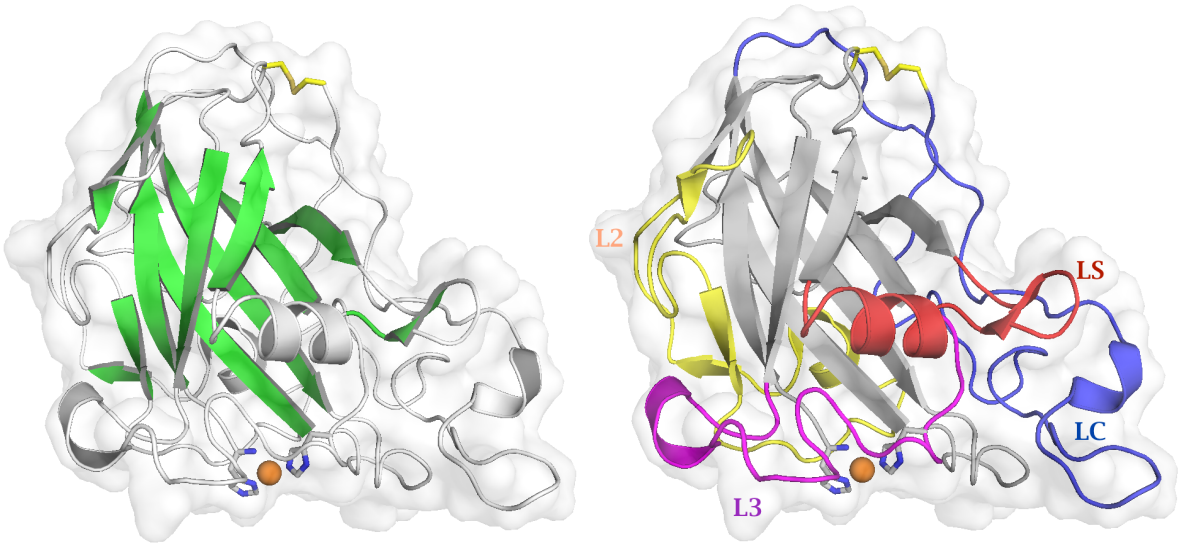

Figure 1.2.1. Crystal structure of a fungal LPMO. The crystal structure belongs to *Neurospora crassa* LPMO9C (PDB id: 4D7U) and shows the common features to LPMOs in general, however, the loops vary greatly between individual LPMOs. The β-sandwich is highlighted in green, and the different loops are colored. The copper ion is always shown as an orange sphere, coordinated by two histidines (shown as sticks).

1.2.3. SUBSTRATE-BINDING SURFACE

The LPMOs have shown activities on various polysaccharides and the majority shows a flat substrate-binding surface that is fit to bind the flat surface of for example cellulose (**Fig. 1.1.2**). There are some exceptions to this generalization, such as the AA13 family (PDB id: 4OPB) that is active on starch and show a rounded binding surface with the active site hidden in a shallow groove (Leggio et al., 2015). Another exception is *Nc*LPMO9C that is active on hemicellulose, indicating that LPMOs are not only active on solid-state substrates such as cellulose and chitin (Isaksen et al., 2014). Altogether, these exceptions challenge our current knowledge of LPMOs.

The substrate-enzyme interactions were already studied in the early work by Vaaje-Kolstad et al. (2005) on CBP21, the chitin-active LPMO10 from *Serratia marcescens* (PDB id: 2BEM; Suzuki et al., 1998) known to be only a chitin-binding module at that time. With the use of site-directed mutagenesis, they showed that the polar amino acids that reside in the flat face and a single aromatic amino acid (located in the L2 loop; Tyr54 in CBP21) were important for substrate binding (Vaaje-Kolstad et al., 2005; Harris et al., 2010) (**Fig. 1.2.2**). A solvent-exposed aromatic residue is very unusual, as hydrophobic amino acid would rather be hidden inside the protein core. The aromatic residue is thought to align with glucose-units to form a

stacking effect due to aromatic-carbohydrate π-CH interactions (Li et al., 2012; Beeson et al., 2015). AA9s have shown to have two or more aromatic residues on the flat face, and the distance and position of these residues corresponds to those of the pyranose units (Li et al., 2012). Cellulose-active LPMOs seems to have a more hydrophobic binding face compared to chitin-active LPMOs, which may reflect the hydrophobic surface of cellulose. All these finding were later confirmed by the obtention in 2016 of an LPMO-oligosaccharide co-crystal, as this was the first study that revealed the substrate-enzyme interaction and establish that LPMO binds to the substrate with its flat surface (Frandsen et al., 2016). The substrate binding site vary greatly between individual LPMOs, whereas the conserved amino acids near the active site is believed to influence the positioning of the active site towards the substrate and contribute to substrate recognition and specificity (**Fig. 1.2.2** and **1.2.3**).

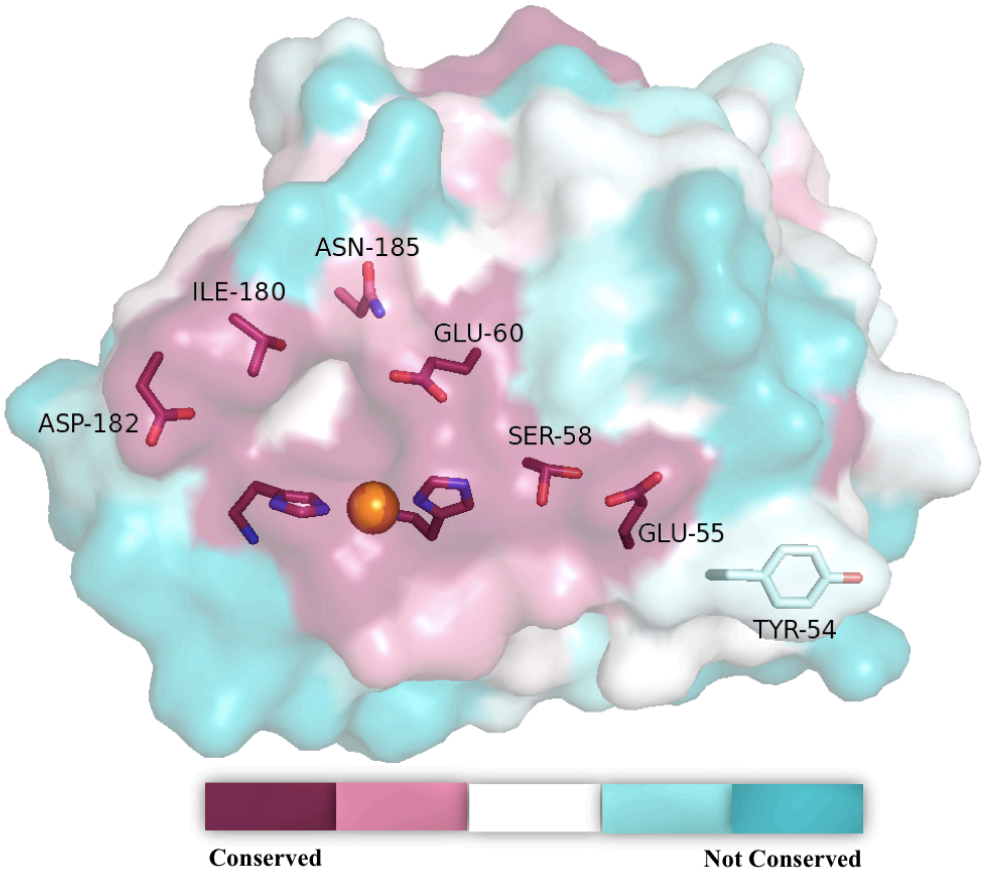

Figure 1.2.2. Substrate-binding site of a chitin-active LPMO. The flat binding surface of the LPMO is faced up, exposing the amino acids involved in substrate binding. Depicting CBP21 (PDB id: 2BEM) that binds to chitin by residues Asp182, Ile180, Asn185, Glu60, Ser58, Glu55 and especially Tyr54. The conserved and non-conserved regions of the protein were calculated through the consurfdb.tau.ac.il/ server, and is colored with a color scale ranging from purple and light pink (most conserved and conserved amino acids) to blue and light blue (least conserved), with the white color in the middle of the color scale. Most of the conserved amino acids lies near the active site. It is worth noting that Tyr54 should have been colored purple, as solvent-exposed aromatic residues are highly conserved and important for substrate binding.

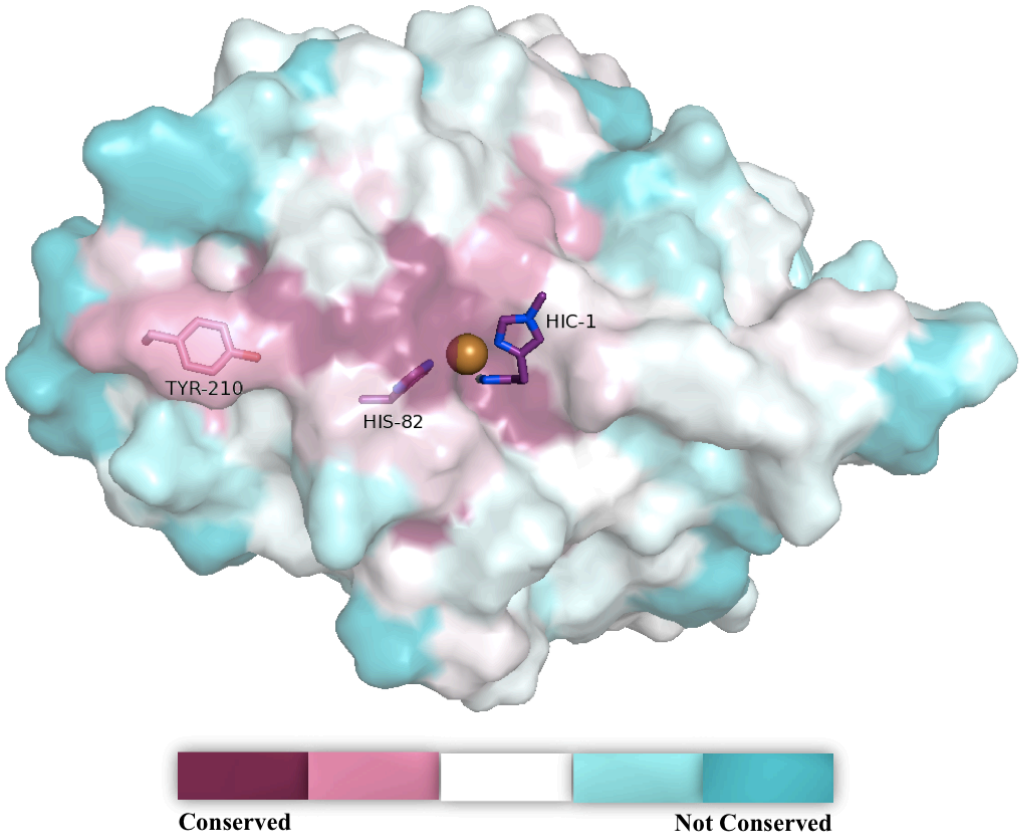

Figure 1.2.3. Substrate-binding site of a cellulose-active LPMO. The flat binding surface of the LPMO is faced up, exposing the Tyr210 involved in binding cellulose. Depicting a LPMO9M expressed from *Neurospora crasse* (PDB id: 4EIS). Data for other amino acids important for binding is currently not available.

Although the majority of family AA10 exists as single domain enzymes, several LPMOs are accompanied with one or more carbohydrate binding modules (CBMs), rich in aromatic amino acid residues, that may reflect substrate preferences (Horn et al., 2012). Closer inspection of the sequences shows that the majority of the appended modules likely promote binding to polysaccharides such as cellulose (CBM1 and CBM2), chitin (CBM1, CBM2, CBM5/12, CBM14 and CBM73) or starch (CBM20) (Vaaje Kolstad et al., 2017). One example is the bi- modular *Streptomyces coelicolor* LPMO, ScLPMO10C (also known as CelS2), which contains a cellulose-binding CBM2 that contributes to activity (Forsberg et al., 2014). When CBM2 is removed, the truncated CelS2-N lost its activity towards cellulose completely due to lack of binding. Surprisingly, the truncated CelS2-N bounded strongly to chitin, showing that the flat face of single domain enzymes can have good binding properties. The activity to LPMOs are fragile to modifications such as removing their natural CBM or introducing CBMs from other proteins, since it often leads to apparent (partial) activity loss, as shown by Crouch *et al.* (2016) and Borisova *et al.* (2015). This loss may be related to

altered proximity with the substrate or to inactivation phenomenon (see section 1.2.6. for further discussion).

Despite recent progress, the structural determinants of LPMO substrate specificity remain largely unknown (Vaaje-Kolstad et al., 2017). The data gathered to date, which describes the binding surface, are insufficient to conclude if and how the mode of substrate-binding affects the oxidative regioselectivity. However, the data show interesting correlations that could be explored further in future structure-function studies.

1.2.4. PROPOSED REACTION MECHANISM

The oxidative properties of LPMOs were first established by Vaaje-Kolstad et al. (2010), when they detected traces of unidentified chitooligosaccharides in reactions carried out with CBP21 in presence of O_2 and reductant. The product was identified as chito-oligosaccharides with an oxidized sugar at the reducing end. Oxidized products indicate an oxidative step. This was determined by experiments performed in $^{18}O_2$ saturated conditions and monitored by MALDI-TOF MS, whereas the oxidized products showed a mass increase of two atomic mass units (amu) compared to those that did not contain isotope-labeled molecular oxygen. Removal of dissolved molecular oxygen in the reaction solution inhibited CBP21 activity, which confirmed the requirement for molecular oxygen for catalysis (Vaaje-Kolstad et al., 2010). A strong indicator for an oxidative step is the complete inhibiting effect of cyanide, a known O_2 mimic, on LPMO. With all the supporting claims done by Vaaje-Kolstad et al. (2010), new families of CAZymes were established and acknowledged by other researchers.

In 2011, Phillips et al. discovered a different kind of oxidized product, showing oxidation on the nonreducing end, and was determined to be 4-ketoaldose by mass spectrometry and later confirmed in an independent study that used two-dimentional NMR (Isaksen et al., 2014). This confirms that LPMOs can perform oxidation on each side of the glycosidic bond, which is in consensus with the context of an intact crystalline structure. Furthermore, the cellulose-active LPMOs have shown different product profiles, showing oxidation on C1, C4 or a mixture of both. Thus, Phillips et al. (2011) proposed to divide them into three main groups: type 1 LPMOs, which oxidize C1; type 2 LPMOs, which oxidize C4; type 3 LPMOs, which can oxidize both C1 and C4. There is also a subset of type 3 LPMOs, termed the LPMO3* subfamily, that appear to have lost C4 activity and can carry out only C1 oxidation.

Additionally, the regioselectivity of oxidation is largely thought to be due to the positioning of a LPMO on a specific substrate, but this is too early to conclude. A study have shown synergy between a C1/C4 oxidizing and a C1 strict LPMO, which is an important finding which warrants further investigation to identify the best enzyme combinations for polysaccharide degradation (Forsberg et al., 2014).

Already in 2011, Phillips et al. proposed a reaction mechanism to LPMOs. They proposed that the copper ion is first reduced from +2 to +1 by a reductant, as reductants have shown to increase the activity in many folds (Vaaje-Kolstad et al., 2010). Cu(I) binds to oxygen (O_2) to form a Cu(II)-superoxo intermediate ($O_2^{\bullet-}$) to activate the oxygen for the upcoming reaction. The oxygen atom closest to the substrate abstracts a proton from either C1 or C4 adjacent to the glycosidic bond, to generate a substrate radical. This substrate radical could recombine with the newfound hydroxyl group to the copper-oxo species, leading to hydroxylating the glucan chain to form the intermediate (**Fig.1.2.4**). After hydroxylation, the glycosidic bond is destabilized and likely broken by an elimination reaction, which may be catalyzed by the LPMO or occur spontaneously (Beeson et al., 2012). This elimination is irreversible because the carbon on the reducing or nonreducing end has been oxidized. None of the intermediates mentioned in the proposed reaction mechanism have been detected so far, thus the proposed mechanism is not fully established. Notably, a Cu(II)-superoxide enzyme species has yet to be spectroscopically characterized (Kjaergaard et al., 2014).

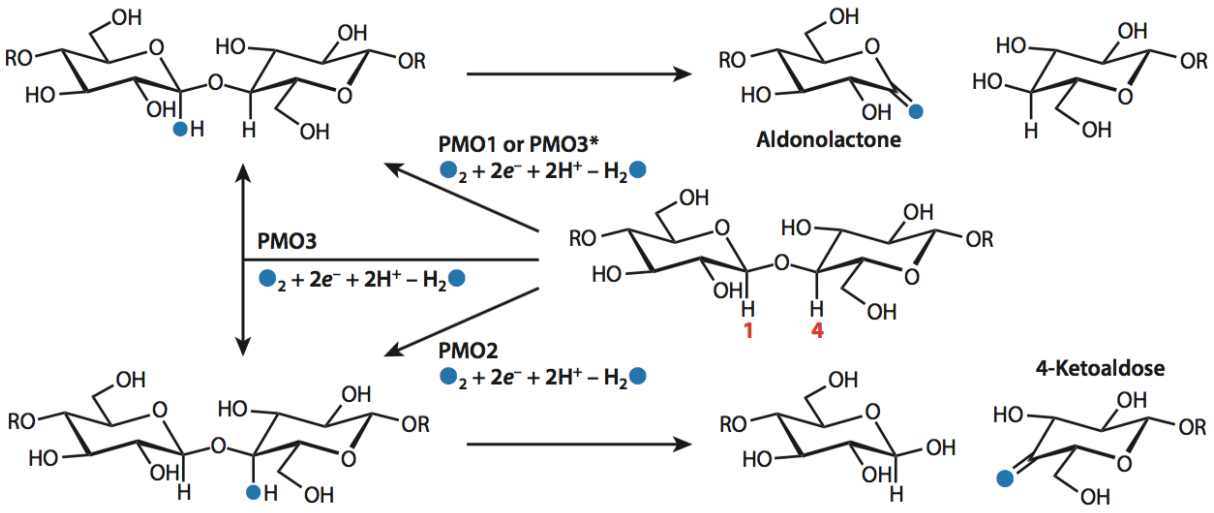

FIGURE 1.2.4. Regioselective oxidation of cellulose by LPMOs. Figure taken from Beeson *et al*., 2015.

1.2.5. ELECTRON DONOR

Hydroxylation of polysaccharides by LPMOs depends on external supply of two electrons; the first electron being necessary to reduce copper and the second one to complete the catalytic cycle imposed by the canonical monooxygenase reaction (**R-H + O_2 + $2H^+$ + $2e^-$ --> --> R-OH + H_2O**) (Phillips et al., 2011). The insensitivity for superoxide dismutase, which catalyzes the conversion of $O_2^{\bullet-}$ to H_2O_2 in the solvent, thus indicating that the activation of oxygen happen inside the active site of LPMOs (Vaaje-Kolstad et al., 2010). A plethora of reducing agents was found to stimulate LPMOs, including ascorbic acid, reducing glutathione (Vaaje-Kolstad et al., 2010), gallic acid (Quinlan et al., 2011), cysteine, pyrogallol (Leggio et al., 2015), resveratrol, catechin, caffeic acid and synaptic acid (Westereng et al., 2015). Interestingly, LPMOs can be activated by lignin that comes in great abundance in lignocellulosic biomass.

Redox enzymes such as bi-modular (FAD-dependent/cytochrome) cellobiose dehydrogenase have shown to stimulate LPMO activity in similar degree as ascorbic acid (Phillips et al., 2011). The challenge with this theory, however, is how the CDH can deliver the two electrons when LPMO is bound to the substrate. A recent NMR study has shown that CDH binds directly on the active site of LPMO (Courtade et al., 2016). Indicating that the electron is stored in the copper ion, however, this is unlikely due to nature of the copper ion (E^0_{ox} = (-)0.15 V). In contrast, Li et al. (2012) suggests that CDH to bind on the side of the LPMO, right above the L2 loop, where several aromatic residues are present, and the electrons are transferred via a conserved hydrogen-bonding network or conserved aromatic residue to the active site. However, no studies have shown this electron transfer.

Cannella et al. (2016) proposed a different approach to reduce LPMOs, with light in the presence of chlorophyllin. Their results showed a 20-fold increase in release of oligosaccharides, compared with no chlorophyllin present. The authors of this study attributed such rate enhancement to some sort of ¨high redox potential¨ electron that would be delivered by photo-excited pigments, although the underlying mechanism was not investigated. Altogether, LPMOs have several natural sources of energy including the lignocellulosic biomass, which facilitate and maintain LPMO activity.

1.2.6. HYDROGEN PEROXIDE AS A CO-SUBSTRATE

During the writing of this thesis, a study with a new perspective on the reaction mechanism was published from our research group. Bissaro et al. (2016) proposed that the co-substrate for LPMOs is in fact hydrogen peroxide. The reaction with LPMO in the presence of a reductant and low concentration of exogenous H_2O_2, showed a significant increase in initial LPMO rates with 26-fold more oxidized products released. This increase in activity corresponds to the increases reported for the reaction with LPMO in the presence of chlorophyllin, light and ascorbic acid (Cannella et al., 2016), thus indicating that H_2O_2 was probably the key element for LPMO activity in this photocatalytic system. To verify the role of H_2O_2 as a co-substrate, isotope labeling was performed with $H_2{}^{18}O_2$ that showed indeed that the oxygen introduced into the polysaccharide chain comes from H_2O_2 and not from O_2. Reactions with lower concentrations of $H_2{}^{18}O_2$ showed that even in the presence of a 10-fold surplus of $^{16}O_2$, the oxidized products carry ^{18}O from $H_2{}^{18}O_2$ and not from $^{16}O_2$. Additionally, a competition experiment with peroxidase and LPMO showed that the peroxidase completely inhibited LPMO activity, despite the presence of O_2 and reductant. Altogether, the experiments showed that H_2O_2 is the catalytically relevant co-substrate for LPMO. Interestingly, these findings might explain why published catalytic rates for LPMOs are low and similar, and, most remarkably, independent of the LPMO or the substrate used (Vaaje-Kolstad et al., 2010; Frandsen et al., 2016; Agger et al., 2014).

The experiments with H_2O_2 indicate strongly that it is the catalytically relevant co-substrate. Thus, Bissaro et al. proposed a new mechanism where H_2O_2 binds to the reduced copper site (LPMO-Cu(I)) and experience homolytic bond cleavage that produce a hydroxyl radical (**Fig.9**). This likely forms a Cu(II)-hydroxide intermediate and a substrate radical by one of several possible pathways. The LPMO remains in the reduced state after reaction, and this was proved when the reactions were added quite low amount of ascorbic acid. Their results showed that product levels are much higher than the total amount of ascorbic acid added. This is in agreement with the proposed mechanism in which a reduced LPMO can catalyze several reactions provided that H_2O_2 is supplied.

Bissaro et al. also observed that at higher H_2O_2 concentrations, the LPMO reactions stopped very rapidly. The inactivation was partly avoided by the presence of substrate. Using proteomics technologies, they observed that the inactivation was due to oxidative damage, especially in the active site. Interestingly, the methylated N-terminal histidine in the active

site of AA9s (Fig. 1.2.3 and Fig. 1.2.6) was one of the most vulnerable to oxidation, which might indicate that the methylation helps protect the fungal LPMOs from oxidative self-destruction. The finding that modifications occurred very locally lead to the conclusion that oxidative damage is not caused by random generation of hydroxyl radical derived from H_2O_2 in solution, but by *in situ* enzyme-generated hydroxyl radicals.

Altogether, this research shed some light into the reaction mechanism of LPMOs, as it explained several unexplained phenomena such as the need for two electrons. With the H_2O_2 as the co-substrate, the recruitment of two electrons and protons is automatically delivered with the co-substrate ($\mathbf{O_2 + 2e^- + 2H^+ = H_2O_2}$). The reaction mechanism, however, still holds mystery over how the active site coordinates the cofactor to perform regioselective oxidation. In the active site, the residues close to the copper ion might shed some light into this matter.

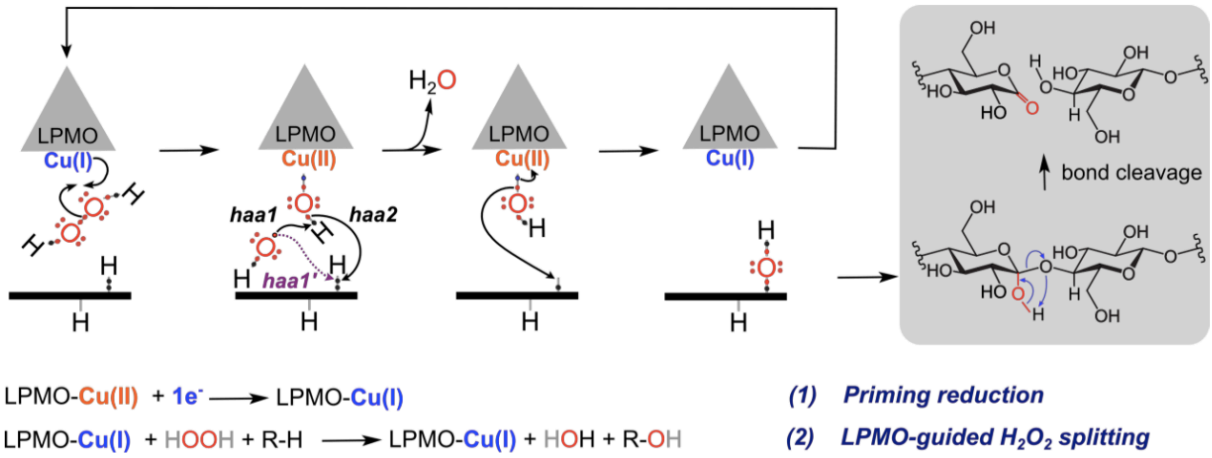

Figure 1.2.5. Proposed reaction mechanism of LPMO using H_2O_2 as the co-substrate. In step one, H_2O_2 binds to the Cu(I) and experience homolytic bond cleavage, resulting a hydroxyl radical. In step two, the hydroxyl radical abstract a hydrogen from either the Cu(II)-hydroxide (haa1) or from the substrate (haa1'). The former scenario generates a copper-oxyl intermediate that can abstract a hydrogen from the substrate (haa2), resulting a substrate radical that bonds to the hydroxyl. Thus, LPMO-Cu(I) is able to catalyze this reaction once again. Figure taken from Bissaro et al., 2016.

1.2.7. ACTIVE SITE

In the active site of LPMOs, the copper ion is tightly bound by three nitrogen ligands contributed by two histidine residues, of which one is N-terminal, in a motif termed the histidine brace (Quinlan et al., 2011; Aachmann et al., 2012). These three N ligands together with a co-substrate form a square plane geometry that is tilted about 30° relative to the binding site plane (Gudmundsson et al., 2014). The histidine brace that coordinates the copper ion is essential for catalysis and is found in all LPMO structures.

When inactive, Cu(II) is coordinated by tyrosine in the axial position (**Fig. 1.2.6)**, a conserved residue for AA9s and also AA11 and AA13. As Cu(II) prefers a coordination number from four to six, the copper coordination sphere is completed with the presence of two water molecules, resulting an octahedral geometry (Karkehabadi et al., 2008; Kjaergaard et al., 2014). On the other hand, the majority of AA10s have a conserved phenylalanine in this position that cause steric hindrance. Together with the axial-positioned alanine (**Fig.1.2.6**), both Phe and Ala provide steric hindrance that results an unusual compressed trigonal-bipyramidal geometry (Vaaje-Kolstad et al., 2012; Hemsworth et al., 2013a; Gudmundsson et al., 2014). The roles of tyrosine and phenylalanine have yet to be fully examined. Furthermore, when Cu(II) is reduced to Cu(I) with a delivery of an electron donor (E^0_{red} = +0.15 V), the copper can only be coordinated be two to four ligands (Beeson et al., 2015), which most likely consist of the co-substrate interacting with the copper ion and forms the plane geometry with the histidine brace. In this case, tyrosine is thought to no longer coordinate the copper ion, and the water molecules are removed to make space for the co-substrate. This transition between Cu(II) and Cu(I) happens with minimal rearrangement of atoms (Kjaergaard et al., 2014).

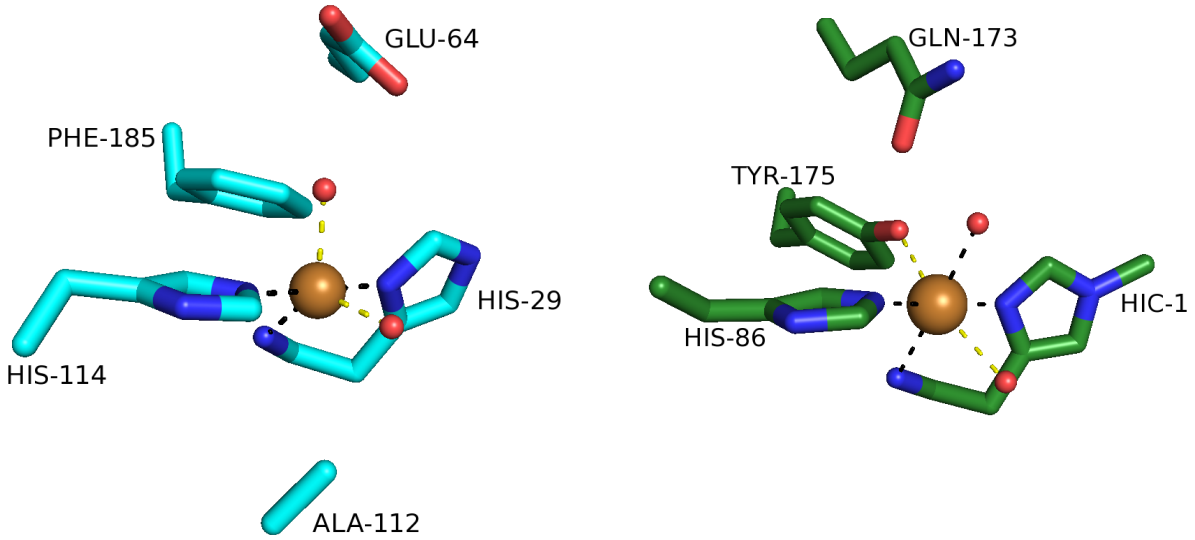

Figure 1.2.6. Active site architecture. The active site to the left (blue) belongs to LPMO10 from *Enterococcus faecalis* (PDB id: 4ALC), displaying a trigonal bipyramidal geometry. The one to the right (green) belongs to LPMO3 from *Thermoascus aurantiacus* (PDB id: 2YET) exhibiting an octahedral geometry. Note that the histidines bind to the copper ion from equatorial positions, while Phe & Ala and Tyr & H_2O (red sphere) lie in the axial position towards the copper ion.

In 2014, Forsberg et al. discovered two highly structurally similar LPMO10s, both from *Streptomyces coelicolor*, with different active site architecture and different oxidative profiles (**Fig. 1.2.7**). *Sc*LPMO10B (PDB id: 4OY6) oxidizes C1/C4 on cellulose with an active site containing an axial tyrosine (Y219), conserved histidine (H214) and glutamine (Q217), which resembles those of fungal LPMOs. On the other hand, CelS2 (PDB id: 4OY7) oxidize C1 exclusively on cellulose with the corresponding residues in the active site of AA10s in general, which are phenylalanine (F219) and glutamate (E217). Interestingly, cellulose-active AA10s, AA11s and AA13s do not appear to show the compressed trigonal bipyramidal geometry but display more typical tetragonal geometry, as observed for AA9s (Forsberg et al., 2014). Notably, *Sc*LPMO10B shows a displacement of the conserved solvent-exposed alanine (A148) compared to the one in CelS2 (A142). Alanine is highly conserved in AA10s and the AA11 enzyme (PDB id: 4MAI), and in the combination with phenylalanine may restrict coordination of copper to only equatorial ligands (Hemsworth et al., 2013b). In C4 oxidizing AA9s, this position appears to be unrestricted, which indicate that alanine might be one of the determining factors for C4 oxidation, including the substrate-binding residues that contributes to positioning the active site according to the substrate. CelS2 is an interesting LPMO, as it resembles those of the chitin-active AA10 enzymes, but manage to be active on cellulose.

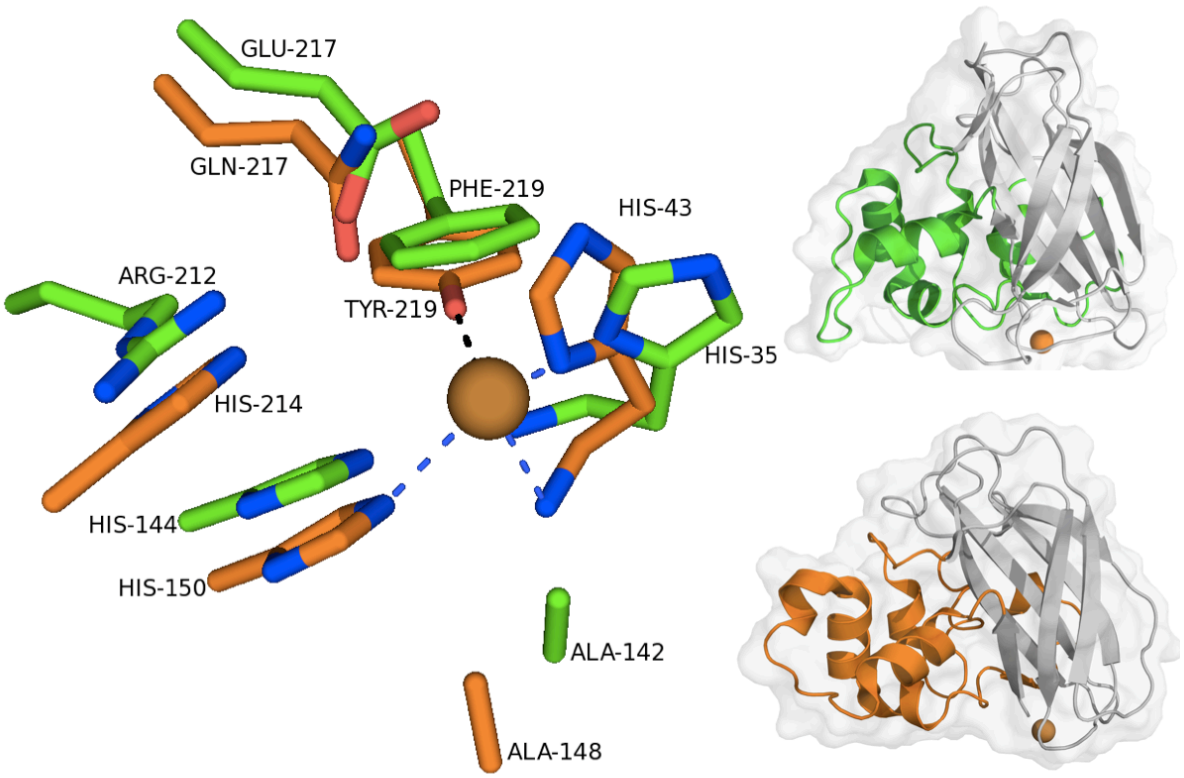

Figure 1.2.7. Structural comparison of CelS2 (PDB id: 4OY7; green) and *Sc*LPMO10B (PDB id: 4OY6; orange). CelS2 have the conserved motif R-X_4-E-X-F while *Sc*LPMO10B have H-X_2-Q-X-Y. The active site architecture to *Sc*LPMO10B resembles those found in the cellulose-active AA9 enzymes.

1.2.8. PURPOSE OF THIS THESIS

Currently, we know the main role of histidines in the histidine brace, where mutation of these histidine residues into alanine and asparagine resulted a completely inactive LPMO (Harris et al., 2010; Vaaje-Kolstad et al., 2005; Loose et al., 2016b). Additionally, we have a pretty good idea of what role alanine, tyrosine and phenylalanine have in the active site (Forsberg et al., 2014b ; Harris et al., 2010), as described in section 1.2.7. However, that is basically all the data we have available about the active site of LPMOs. Thus, there is need for fundamental work to unravel the molecular mechanism of LPMOs and how they can be exploited in biotechnological processes. Thus, the purpose of this thesis is to investigate the roles of glutamate and arginine in CelS2, which lies in close proximity to the copper ion (**Fig. 1.2.7**). CelS2 have been used as a model enzyme for several other studies (Forsberg et al., 2014; Bissaro et al., 2016) and thus some fundamental knowledge of CelS2 is available, which can be used for interpreting the function of Glu217 and Arg212.

CelS2 presents an interesting exception for cellulose-active LPMOs, because - as other cellulose-active LPMOs have tyrosine (Tyr219), glutamine (Gln217) and an additional histidine residue (His214) in the active site (*Sc*LPMO10B numbering; **Fig. 1.2.7**) - CelS2 have phenylalanine (Phe219), glutamate (Glu217) and arginine (Arg212) in the active site, which resembles those of chitin-active LPMOs (**Fig. 1.2.6**). This difference indicates that the active site do not determine substrate specificity, and especially, that these residues can be exchanged (for example Glu219 <=> Gln219) and most likely still contribute to LPMO activity. To test this hypothesis, we used site-directed mutagenesis to make the mutant Glu217Gln and Arg212Lys in CelS2. The additional histidine (His214) in *Sc*LPMO10B is thought to stabilize the second histidine (His144) in the histidine brace by a stacking effect, and the guanidinium group to arginine is thought to function in the same way due to its planar geometry with the three amino groups. Then, by mutating arginine into lysine - a flexible carbon chain with only one amino group - we might eliminate the stacking effect.

Furthermore, the function of Glu217 was further studied by mutating it into aspartate, asparagine and alanine. Both aspartate and asparagine have a shorter carbon chain (one -CH_2- less), which positions the polar side-group further away from the copper ion. Glu217Ala removes glutamate completely and can help to determine if glutamate is important for catalysis at all. Additionally, a double mutant of Glu217Gln//Phe219Tyr in CelS2 was made to resemble the active site of other cellulose-active LPMOs, which was part of an earlier experiment in this thesis that involved *Sc*LPMO10B and its mutant Gln217Glu//Tyr219Phe. Altogether, the effect of mutation was examined by enzyme activity assay (referring to section 3.3.2) and the oxidized products were quantified on ion exchange chromatography after hydrolysis of an endoglucanase (*Tf*Cel5A). These mutations provide major changes into the active site in CelS2, thus we expect to observe a change in activity.

Additionally, the CelS2 variants were run in reaction assay without the substrate to quantify the amount of H_2O_2 produced, as LPMOs are widely known to produce H_2O_2 when the substrate is not present (Bissaro et al., 2016). In the proposed reaction mechanism to Phillips et al. (2011), the copper ion binds to oxygen to form the intermediate Cu(II)-superoxide ($O_2^{\bullet-}$). We want to investigate whether (i) the superoxide is released from the active site and catalyzed by superoxide dismutase (SOD) into H_2O_2, or (ii) the superoxide is protonated inside the active site to produce H_2O_2.

2. MATERIALS

TABLE 2.1. Laboratory Equipment

EQUIPMENT	SPECIFICATION	SUPPLIER
Autoclave tape	18 mm 12 mm	VWR
Automatic pipettes,	Finnpipette F2 Pipettes, single channel pipettes	Thermo Scientific
Balancers	Sartorius basic	Sartorius
Biosafety cabinets	Av-100	TelStar
Blue-cap bottles	1000 mL, 500 mL, 250 mL, 100 mL	VWR
Blue-cap tubes	Cellstar® tubes 50 mL 15 mL	Greiner Bio-One
Centrifuge	Avanti™ J-25 Sentrifuge - 5430R	Beckman Eppendorf
Centrifuge rotors	JA10	Beckman
Centrifuge tubes	500 mL 25 mL	Nalgene
Centrifugal filters for protein concentration	Amicon Ultra-15 10K, pink cap	Merck Millipore
LP Chromatographic system	BioLogic LP system BioFrac Fraction Collector	Bio-Rad
Cryotubes	2 mL	Sarstedt
Culture flasks	2000 mL	Nalgene
Culture tubes, green cap	15 mL	VWR
Electrophoresis equipments	Vertical electrophoresis tank Power supply	VWR
Eppendorf tubes	1,5 mL - Axygen®	VWR
Filters	Steritop™ 0,22 µm	Millipore

Filter plate, 96 wells		Millipore
Freezer (-20°C)		Bosch Whirlpool
Freezer (-80°C)	Ultra-Low	SANYO
Fume hood	Mc6	Waldner
Gel imager	Gel Doc EZ Imager	Bio-Rad
Glass equipment		Schott-Duran/ VWR
Gold electrode, PAD detection	Disposable Electrode Dionex Carbohydrate Certified	Thermo Scientific
HiTrap DEAE FF	5 mL	GE Healthcare
HiLoad™16/600		GE Healthcare
Superdex™ 75 Prepgrade		
HPLC-columns	Dionex™ CarboPac™ PA1 Analytical and Guard column	Thermo Scientific
HPLC system	ICS 3000	Thermo Scientific
Ice maker	KF 145	PORKKA
Incubator		Termaks
Inoculation loops	1 µL	Sarstedt
Magnetic stirrer		VWR
Microbalance	Sartorius CP-2P	VWR
Multiskan™ FC Microplate Photometer		Thermo Scientific
Parafilm	5 cm	VWR
Pasteurpipettes	Plastic, 5 mL	VWR
PCR cooler		Eppendorf
PCR system	PCR Doppio SimpliAmp	VWR Thermo Scientific
PCR tubes	0,2 mL	VWR
Petri dish	9 cm	Heger
pH benchtop meter	FiveEasy Plus	Mettler Toledo Sentron
Pipette tips	Next Generation Tip Refill	VWR
Refrigerator (4°C)		Whirlpool
Shaking incubator	Multitron HT	Infors

Size Exclusion Chromatography	HiLoad™ 16/60 Superdex™ 75 prep grade	GE Healthcare
Sonicator bath	Transonic 460/H	Elma
Spectrophotometer	AG Biophotometer	Eppendorf
	WPA CO8000 Cell Density Meter	Biochrom
Syringe filters	0,20 µM	Sarsted
Syringes	50 mL, 30 mL, 20 mL, 10 mL, 2 mL, 1 mL	BD-plastipak
Table top centrifuge	Sigma 1-14	LABEX
Thermomixer	Comfort	Eppendorf
	C	Eppendorf
Ultrasound bath	Transsonic 460/H	Elma
Uvettes	1 x 1 cm	Eppendorf
Vacuum manifold		Millipore
Vortex	Vortex-2 Genie	Scientific Industries
	MS 3 basic	IKA
Water bath	Eco Temp TW12	Julabo
Weighing boats		VWR
Whirlmixer	Vortex-Genie 2	Scientific Industries
	MS 3 Basic	IKA
Qubit fluorometer		Life Technologies

TABLE 2.2. Softwares for Analysis

SOFTWARE	APPLICATION	SUPPLIER
Chromeleon Chromatography Studio	HPLC	Chromeleon
CLC DNA Workbench	Sequencing	CLCbio
ExPASy ProtParam tool	Calculations of pI, MW and ε	ExPASy
ImageLab	Gel visualization	BioRad
LP Data View	LP-chromatographic system	BioRad
QuikChange primer design tool	Primer design	Agilent Technologies
SkanIt	Multiskan^{TM} FC Microplate Photometer	Thermo Scientific

TABLE 2.3. Chemicals

CHEMICAL		SUPPLIER
Acetic acid	CH_3COOH	Sigma-Aldrich
Agar -agar		Merck Millipore
Ampicillin sodium salt	$C_{16}H_{18}N_3NaO_4S$	Sigma-Aldrich
Amplex® Red reagent (10-acetyl-3,7-dihydroxyphenoxazine)	$C_{14}H_{11}NO_4$	Thermo Scientific
Avicel® PH-101, cellulose microcrystalline		Sigma-Aldrich
Bacto^{TM} Yeast Extract, granulated		Merck
Bacto^{TM} Tryptone (peptone from casein)		Merck
Bis-Tris methane	$C_8H_{19}NO_5$	VWR
Coomassie® Brilliant Blue R-250		Bio-Rad
Dimethylsulfoxide (DMSO)	$(CH_3)SO$	Thermo Scientific
Distilled water, dH_2O (Milli-Q quality)		Merck Millipore
Ion-free water, FLUKA TraceSELECT®		Sigma-Aldrich
Ethylenediaminetetraacetic acid (EDTA)	$C_{10}H_{16}N_2O_8$	Sigma-Aldrich
Ethanol	C_2H_5OH	VWR
Glycerol	$C_3H_5O_3$	VWR
Hydrogen chloride	HCl	Sigma-Aldric

Isopropanol	C_3H_8O	VWR
L-ascorbic acid	$C_6H_8O_6$	Sigma-Aldrich
Magnesium chloride	$MgCl_2$	VWR
NuPAGE® 10% Bis-Tris Gel 1,0 mm x 10 wells		Life Technologies
NuPAGE® LDS Sample Buffer (4x)		Life Technologies
NuPAGE® Reducing Agent (10x)		Life Technologies
NuPAGE® MES SDS Running Buffer (20x)		Life Technologies
Protease inhibitor cocktail tablets		Sigma-Aldrich
SOC media		Life Technologies
Sodium acetate	$NaCH_3COOH$	Sigma-Aldrich
Sodium hydroxide	NaOH	VWR
Sodium chloride	NaCl	
Sodium phosphate dibasic	$H_2NaO_4P * 2H_2O$	Sigma-Aldrich
Sodium phosphate monobasic	$HNa_2O_4P * H_2O$	Sigma-Aldrich
Trizma base	$C_4H_{11}NO_3$	Sigma-Aldrich
Tryptone		Merck Millipore
Yeast extracts		Merck Millipore

TABLE 2.4. Self-made Media and Buffer

MEDIA	CONTENT
LB media	10 g Tryptone 5 g Yeast 10 g NaCl Add dH_2O to 1 L volume, and adjust the pH to 7,0-7,5 with 6 M NaOH. Lastly, autoclave the solution.
LB media with Agar agar 100 µg/mL ampicillin	10 g Tryptone 5 g Yeast 10 g NaCl 15 g Agar agar Add dH_2O to 1 L volume, and adjust the pH to 7,0-7,5

	with 6 M NaOH. Autoclave the solution, and when the solution has cooled down to ~50°C, add 1 mL of 100 mg/mL ampicillin in a biosafety cabinet. Lastly, pour the solutions into petri dishes before they solidifies. Store them at 4°C.
Spheroplast Buffer	10 mL 1 M Tris-HCl, pH 8.0 17.1 g Sucrose 100 µL EDTA pH 8.0 1 cOmplete™ Protease Inhibitor Cocktail Tablet, from Roche Add ice-cold dH_2O to 100 mL

TABLE 2.5. Kits

KIT	CONTENT	SUPPLIER
Amplex® Red Hydrogen Peroxide/ Peroxidase Assay Kit	5 x reaction buffer (0.25 M sodium phosphate, pH 7.4) Amplex® Red (154 µg) Dimethylsulfoxide (DMSO) 10 U Horseradish peroxidase (HRP)* Hydrogen Peroxide (H_2O_2)	Molecular Probes (Thermo Scientific)
E.Z.N.A.® Plasmid Mini Kit I, V(capped) spin	**Solution I** (50 mM Tris-HCl pH 8.0, 10 mM EDTA, 100 µg/mL RNaseA) **Solution II** (200 mM NaOH, 1% SDS) **Solution III** (4.2 M Guanidine-HCl, 0.9 M potassium acetate pH 4.8) **Equilibrium Buffer** (3 M NaOH) **HBC Buffer** (5 M Guanidine-HCl, 30% isopropanol) **DNA Wash Buffer** (10 mM Tris-HCl pH 7.5, 80% ethanol) **Elution Buffer** (10 mM Tris-HCl, pH 8.5) **HiBind™ DNA mini columns** **Collection tubes** (2 mL)	Omega BIO-TEK

Pellet Paint® Co-Precipitant	Pellet Paint® Co-Precipitant 3 M Sodium acetate, pH 5,2	Novagen
Qubit® dsDNA BR Assay Kit	Qubit® dsDNA BR Reagent (Dimethyl sulfoxide, x200) Qubit® dsDNA BR Buffer (Tris-EDTA, buffer)	Life Technologies
QuikChange II Site-Directed Mutagenesis Kit	PfuUltra High-Fidelity DNA polymerase (2.5 U/ µl)* 10x reaction buffer *DpnI* restriction enzyme (10 U/µl)* dNTP mix	Agilent Technologies

* ¨1 unit (U) is defined as the amount of enzyme that will form 1.0 mg purpurogallin from pyrogallol in 20 seconds at pH 6.0 and 20 ^{0}C¨ (ThermoFisher Scientific, 2017).

TABLE 2.6. Bacteria Strain

BACTERIA STRAIN	SPECIFICATION	SUPPLIER
Escherichia coli One Shot® BL21 Star™ (DE3)	Chemical competent cells for protein expression	Life Technologies

TABLE 2.7. CelS2 wild-type (WT) and selected Point Mutations on CelS2

ENZYME	SPECIFICATION	SUPPLIER
Lytic polymerase monooxygenases (LPMOs)	***Sc*LPMO10C-WT** *Sc*LPMO10C-R212K *Sc*LPMO10C-E217Q//F219Y *Sc*LPMO10C-E217Q *Sc*LPMO10C-E217D *Sc*LPMO10C-E217N *Sc*LPMO10C-E217A	Self-produced
BenchMark™ Protein Ladder		Life Technologies

TABLE 2.8. Primers used for QuikChange II Site-Directed Mutagenesis to Incorporate the Desired Mutation on the Gene Encoding CelS2

The mutated codons that express the desired amino acid are shown as boldface letters. The primers were designed by Postdoc Anne Grethe Hamre, and were made by Invitrogen (Thermo Fisher Scientific). ¨fw¨ stands for forward primers; and ¨rev¨ for reverse primers.

Primers	5' to 3'
CelS2_R178K_fw	GAAAAAGTTTTCTTGAGAGTCGCT**CTT**CACCCACTGCATAAAAATCAGAGC
CelS2_R218K_rev	GCTCTGATTTTTATGCAGTGGGTG**AAG**AGCGACTCTCAAGAAAACTTTTTC
CelS2_E217Q//F219Y_fw	CACATCGGAGCAACTGAA**ATA**GTT**CTG**TTGAGAGTCGCTGCGCACC
CelS2_E217Q//F219Y_rev	GGTGCGCAGCGACTCTCAA**CAG**ACC**TAT**TTCAGTTGCTCCGATGTG
CelS2_E217Q_fw	ACATCGGAGCAACTGAA**ATA**GTTTTCTTGAGAGTCGC
CelS2_E217Q_rev	GCGACTCTCAAGAAAAC**TAT**TTCAGTTGCTCCGATGT
CelS2_E217D_fw	GAGCAACTGAAAAAGTT**ATC**TTGAGAGTCGCTGCG
CelS2_E217D_rev	CGCAGCGACTCTCAA**GAT**AACTTTTTCAGTTGCTC
CelS2_E217N_fw	AGCAACTGAAAAAGTT**ATT**TTGAGAGTCGCTGCGCACCCAC
CelS2_E217N_rev	GTGGGTGCGCAGCGACTCTCAA**AAT**AACTTTTTCAGTTGCT
CelS2_E217S_fw	GGAGCAACTGAAAAAGTT**TGA**TTGAGAGTCGCTGCGCACC
CelS2_E217S_rev	GGTGCGCAGCGACTCTCAA**TCA**AACTTTTTCAGTTGCTCC
CelS2_E217A_fw	AGCAACTGAAAAAGTT**TGC**TTGAGAGTCGCTGCGC
CelS2_E217A_rev	GCGCAGCGACTCTCAA**GCA**AACTTTTTCAGTTGCT

TABLE 2.9. Sequencing Primers

Sequencing primers are used to verify that the desired mutation was incorporated on the pRSET B_*cels2* vector after Site-Directed Mutagenesis. The primers were designed by Postdoc Anne Grethe Hamre, and were made by Invitrogen (Thermo Fisher Scientific) ¨fw¨ stands for forward; and ¨rev¨ for reverse primers.

	5' to 3'
CelS2_seq_391_fw	TGGGATGACCTGGAACTGAT
CelS2_seq_573_rev	CACATCGGAGCAACTGAAAA
CelS2_seq_697_fw	GCCGTCTATAGCGTGGAAAA
CelS2_seq_852_rev	ACTGTTCAGTGAGCCATTCC

3. METHODS

3.1. SITE-DIRECTED MUTAGENESIS

Site-directed mutagenesis (SDM) creates site-specific mutation in the double-stranded vector such as insertion, deletions and point mutations (Agilent Technologies, 2017). Thus, is an invaluable technique for characterizing the relationship between the protein structure and its function. For this purpose, pRSET B bacterial expression vector containing the gene encoding CelS2 (*Sc*LPMO10C residues 35-364, Uniprot ID; Q9RJY2) from *Streptomyces coelicolor* was used, which was cloned in by Zarah Forsberg beforehand (Forsberg et al., 2014, supplements). Before performing site-directed mutagenesis, the pRSET B_*cels2* vector was isolated with the protocols described in section 3.1.1 and 3.1.2, and then, used as basis for mutagenesis together with designed oligonucleotide primers to confer the desired mutations (shown in Table 2.7). The pRSET B_*cels2* with the desired mutation was transformed into BL21 Star (DE3) chemically competent *E.coli* cells by heat shock, which display properties of high-level of protein expression (Thermo Scientific, 2017).

3.1.1. CULTIVATING CELLS IN SMALL VOLUMES

Materials:

- Cryotubes with transformants
- LB agar plates supplemented with ampicillin (100 μg/mL)
- LB media
- 100 mg/mL ampicillin

Method:

The pRSET B_*cels2* was previously transformed into BL21 Star (DE3) chemically competent *E.coli* cells by Zarah Forsberg and stored in cryotubes in -80 °C (Forsberg et al., 2014, supplements). Before cultivating in small volumes, the frozen cells were streaked on agar plates with LB-media and incubated over night (O/N; ~16-20 h) at 37 °C. Inside biosafety cabinets, one single colony was picked from the freshly-streaked agar plate with a sterile wooden toothpick and dropped into each culture tubes, containing 4 mL LB media and 2 μL 100 mg/mL Ampicillin (final concentration 100 μg/mL Amp). The culture tubes were incubated at 37 °C with vigorous shaking (200 rpm) in 12-16 hours.

3.1.2. ISOLATING PLASMID

Materials:

- Cell culture
- E.Z.N.A.® Plasmid Mini Kit I, V(capped) Spin Protocol

Method:

The plasmid was isolated with the E.Z.N.A.® Plasmid Mini Kit I, which disperses the cells by alkaline lysis and separates the plasmid DNA from genomic DNA (OMEGA biotek, 2017). First, 1.5-4.5 mL of cell culture was spun down in 1.5 mL eppendorf tube at 10,000 x g in one minute. The culture media was decanted. The cell pellet was resuspended with 250 µL Solution I with RNase A, and then added 250 µL Solution II to undergo a lysis reaction. The reaction went for 2 minutes, before adding 350 µL Solution III and immediately invert the tube several times to form a flocculent white precipitate. Then, centrifuged at 13,000 x g for 10 minutes to get a compact white pellet.

The next part of the protocol involves purifying the plasmid. The HiBind® DNA Mini Column was inserted into a 2 mL Collection Tube, equilibrated with 100 µL Equilibrium buffer and then centrifuge at 13,000 x g for one minute. Discard the filtrate and reuse the collection tubes after every step until the last step involving elution of plasmid. The supernatant was transferred to the HiBind® DNA Mini Column without disturbing the compact white pellet. Centrifuged at 13,000 x g for one minute. The plasmid is bound to the column matrix. The column was washed with 500 µL HBC Buffer diluted with Isopropanol, centrifuged, added 700 µL DNA Wash Buffer diluted with Ethanol and centrifuged again. The empty column was centrifuged for 2 minutes to dry the column matrix. The column was transferred to a clean 1.5 mL eppendorf tube, added 30 µL Elution Buffer to collect the plasmid and centrifuged for the last time for one minute. The isolated plasmid was stored at -20 °C.

3.1.3. DETERMINING DNA CONCENTRATION

Materials:

- Qubit® dsDNA BR Assay Kit
- Isolated plasmid (referring to paragraph 3.1.2)

Method:

The concentration of isolated plasmid was determined with Qubit® dsDNA BR (Broad-Range) Assay Kit and a Qubit® Fluorometer, which measures from 100 pg/µL to 1000 ng/µL DNA (Thermo Fischer Scientific, 2017). A working solution was made of n x 9 µL BR reagent and n x 199 µL BR buffer, whereas n is the number of samples that to be measured, and 198 µL was distributed to each Qubit® assay tubes with 2 µL of isolated plasmid. The samples were vortexed and incubated at room temperature for two minutes, and then measured in the fluorometer with a standard curve. It is recommended to use three parallels.

3.1.4. PRIMER DESIGN

The mutagenesis requires two primers, one forward primer and one reverse primer, each containing the desired mutation. The oligonucleotide primers, each complementary to the opposite strands of the vector, are extended during temperature cycling by DNA Polymerase Agilent Technologies, 2017). The designed primers should to be 25-45 base pairs long with the point mutation in the center, The primers ends need to be rich with GC-nucleotides to stabilize the binding with the vector. Lastly, the melting temperature should be $\geq$ 78 °C and this can be accomplished by keeping the content of GC-nucleotides higher than 40%. The formula to calculate the melting temperature is given by the instruction manual to Agilent Technologies. The mutagenic primers, shown in Table 2.10, were designed with the use of the web-based QuikChange Primer Design Program from Agilent Technologies.

3.1.5. POLYMERASE CHAIN REACTION AND *DpnI* DIGESTION

Polymerase chain reaction (PCR) performs thermal cycling and amplifies DNA in vitro with the help of a DNA Polymerase. PCR runs in three steps; denaturation, hybridization and extension. In denaturation, the sample is warmed up to 95 °C to denature the template to single-stranded DNA. In the next step, hybridization, the temperature is reduced to 55 °C to let the primers attach to the vector. Lastly, the temperature arises to 68 °C, which is the temperature optimum to *PfuUltra* High-fidelity DNA polymerase, and the primers are extended to form new vectors with the desired mutation (Agilent Technologies, 2017; Mathews et al, 2013). The cycle of these steps are repeated over and over again to create large amount of the mutated vector.

Materials:

- QuikChange II Site-Directed Mutagenesis Kit.
- Template: Isolated plasmid (referring to paragraph 3.1.2)
- Primers (referring to Table 2.8)

Method:

The solutions used for making the sample reactions, shown in Table 3.1.1, are provided by the QuikChange II Site-Directed Mutagenesis Kit. The sample reactions were prepared in PCR tubes on a PCR cooler, but *PfuUltra* DNA polymerase was added right before starting the PCR program, shown in Table 3.1.2. The time length for extension is determined by the size of the template, which 1 kilobases (kb) of plasmid length requires 1 minute at 68 °C per cycle. The pRSET B_*cels2* vector is 4.0 kb long, thus requires 4 minutes to produce complete vectors with mutated *cels2*. After the PCR reaction, the sample was added 1 µL *DnpI* and incubated at 37 °C for an hour, which is an endonuclease that recognize and degrades hemi-methylated and methylated DNA, to remove nonmutated DNA (Agilent Technologies, 2017).

TABLE 3.1.1. Content of sample reaction for the QuikChange II SDM Method.

Reagent	**Amount**
10x reaction buffer	5 µL
dsDNA template	X µL (75-100 ng)
Forward primer	1.25 µL (125 ng)
Revers primer	1.25 µL (125 ng)
dNTP mix	1 µL
dH_2O	until the total volum is 50 µL
PfuUltra DNA Polymerase	1 µL (i.e. the total volum is 51 µL)

TABLE 3.1.2. Cycling Parameters for the QuikChange II SDM Method

Cycle step	Numbers of cycles	Temperature	Time
Heating	x1	110 °C	
Initial denaturing	x1	95 °C	0.5 min
Denaturing		95 °C	0.5 min
Hybridization	x 18	55 °C	1.0 min
Extension		68 °C	X*
Cooldown	x1	10 °C	

* The time length for extension is 1 minute per kilobases of plasmid lenght.

3.1.6. PURIFYING PLASMID

Materials:

- *DnpI*-treated reactions (referring to paragraph 3.1.5)
- Pellet Paint® Co-Precipitant Kit
- 3 M NaAc
- 70% ethanol
- Ethanol (absolute, 100%)
- Autoclaved dH_2O

Method:

Before transforming the mutated plasmid into competent cells, in paragraph 3.1.7, the plasmid was purified with the Pellet Paint® Co-Precipitant Kit. This kit involves precipitating the plasmid to remove primers and other impurities in the sample (Merck Millipore, 2017). The *DnpI*-treated reaction was transferred to eppendorf tubes, then added 2 µL Pellet Paint® Co-Precipitant, 0.1 volumes 3M Sodium Acetate and two volumes of Ethanol (100%, absolute ethanol). The sample was incubated in two minutes to precipitate the plasmid, and then centrifuged at 16,000 x g in several minutes to form a pink pellet. The supernatant was removed. The pink pellet was washed with 5 volumes of 70% ethanol and centrifuged anew. Decanted and 5 volumes of Ethanol were added for a final wash and centrifugation. Decanted and the lid to the eppendorf tubes was let open to evaporate the rest of Ethanol. Any remaining Ethanol can destroy the competent cells under the transformation. Lastly, the pink pellet was resuspended 5 µL sterile dH_2O.

3.1.7. TRANSFORMING COMPETENT CELLS WITH MUTATED PLASMID

Materials:

- One Shot® BL21 Star™ (DE3) chemical competent *E.coli*
- Purified PCR product (referring to 3.1.6)
- SOC-media
- LB agar plates supplemented with ampicillin (100 µg/mL)
- 100 mg/mL Ampicillin

Method:

The PCR product was transformed into One Shot® BL21 Star (DE3) chemical competent *E.coli* cells, which are appropriate to protein expression. The competent cells were thawed on ice, and then added all 5 µL of the *DnpI*-treated reaction and incubated on ice for 30 minutes. The competent cells underwent a transformation when incubated in a preheated water bath at 42 °C in approximately 30 seconds and then set on ice for 2 minutes. The transformants were added 250 µL SOC media, produced by Life Sciences, and incubated in an hour. At last, the transformants were distributed on two agar plates with LB media and Amp (100 µg/mL), one with 150 µL culture and the other with 50 µL. The remaining 50 µL culture was incubated with 0.5 µL Amp O/N. In the next day, if no transformants were observed, the remaining 50 µL culture was also plat out.

3.1.8. SEQUENCING

Materials:

- Cell cultures of new transformants
- 87% glycerol
- Isolated plasmid (80-100 ng/µL) (referring to paragraph 3.1.2)
- Sequencing primers (5 pmol/µL) (Table 2.9)

Method:

To verify that the transformants have incorporated the desired mutation and no random mutations have happened, the isolated plasmids were sent for sequencing at GATC Biotech (Konstanz, Germany). First, the transformants were cultured in small culture volumes, in the same manner as in paragraph 3.1.1, and the mutated plasmids were isolated with the E.Z.N.A Plasmid Miniprep kit I Spin protocol, referring to paragraph 3.1.2. Cryotubes with each

transformants were made with 1050 µL cell culture and 450 µL autoclaved 87% glycerol. The samples for sequencing were prepared by adding 5 µL isolated plasmid (preferably 80-100 ng/µL) and 5 µL sequencing primer (100 ng/µL) in eppendorf tubes. Four parallels were made with four different primers. The tubes were marked with Barcodes so the results of sequencing are delivered to the right owner.

3.2. EXPRESSION AND PURIFICATION OF LPMO

Materials:

- Cryotubes with transformants
- LB media
- 100 mg/mL ampicillin

Method:

BL21 Star (DE3) cells harboring the pRSET B vector with wild-type and mutated *cels2* were grown at 37 °C with vigorous shaking (200 rpm) to an OD_{600} = 0.6 (~20 h) in LB media supplemented with 100 µg/mL Amp. The cells were harvested by centrifugation with JA10 rotor at 8000 rpm and 4°C for 15 minutes. The cells can be stored at -20 °C until further preparations.

3.2.1. PERIPLASMIC EXTRACTION

Materials:

- Cell pellet (referring to 3.2)
- Spheroplast buffer
  - 10 mL 1 M Tris-HCl pH 8.0
  - 17.1 g sucrose
  - 100 µL 0.5 M EDTA pH 8.0
  - 1 cOmplete™ Protease Inhibitor Cocktail Tablet, from Roche
  - Add ice-cold dH_2O to 100 mL
- 20 mM $MgCl_2$
- Ice-cold dH_2O

Method:

The pRSET B_*cels2* vector contains a signal peptide that signals translocation of CelS2 out from the cytoplasm to the periplasmic space in *E.coli*, between cytoplasmic membrane and outer membrane. The proteins were released from the periplasmic space by cold osmotic shock, with a cold spheroplast buffer with high concentration of sucrose, which removes the outer layer. The cells take up the sucrose, and by exposing them to dH_2O and $MgCl_2$ afterwards, forces the cells to experience osmotic shock.

First, the cell pellets were resuspended in a spheroplast buffer and distributed in four 25 mL centrifuge tubes. The tubes were incubated on ice for five minutes before centrifuging at 8000 rpm, 4 °C for 10 min. The supernatant was removed, and the pellets were incubated at room temperature in 10 min. Ice-cold dH_2O (75 mL) was distributed to the four tubes and the cell pellets resuspended. Incubated on ice in 45 seconds before adding 625 µL 20 mM $MgCl_2$ and centrifuged again. The supernatant was filtrated and stored at 4 °C until further purification.

Before the next step, referring paragraph 3.2.2, the protein solution must be adjusted to 50 mM Tris-HCl pH 7.5, by adding 75 mL of this buffer. The pH of the protein solution was adjusted to pH 7.5 by carefully adding drops of diluted HCl, as the proteins can be precipitated by the local drastic change of pH. The protein solution was filtrated again.

3.2.2. ANION EXCHANGE CHROMATOGRAPHY

Materials:

- Sterile filtrated protein solution pH 7.5 (referring to paragraph 3.2.1)
- HiTrap™ DEAE FF, 5 mL bed volume
- Buffer A: 50 mM Tris-HCl pH 7.5
- Buffer B: 50 mM Tris-HCl pH 7.5, 0.5 M NaCl
- 20% ethanol

Method:

The first purification step to isolate CelS2 was done by high performance anion exchange chromatography (HPAEC) and monitored by Ultraviolet detection, using a HiTrap™ DEAE FF column operating with a flow rate of 3.5 mL/min in 50 mM Tris-HCl pH 7.5 (Buffer A).
The column is a weak anion exchanger with tertiary ammonia groups (diethylaminoethyl, DEAE) (GE Healthcare, 2017). Negatively charged proteins bind to the positively charged tertiary ammonia groups in the column, and by increasing the ion concentration with NaCl forces the proteins to elute. First, the column washed with buffer A for 5 min (i.e. four column washes) and 100% buffer B for 5 min to remove leftovers of impurities in the column before applying the sample. The eluted proteins are detected by the UV detector, because the aromatic amino acids phenylalanine, tyrosine and tryptophan absorb UV radiation, and are shown as peaks in the chromatogram. Then the column was equilibrated with buffer A in

5 min before the protein solution was applied and the void collected. When the UV-baseline was stable again, a linear gradient of 0-100% B over 100 min was run. Proteins with a weak negatively charged surface are eluted first, while proteins with more negative charges on the surface are eluted later on the gradient. The elution gradient was collected in fractions of 7 mL (50 fractions in total), and the fractions of interest were analyzed on SDS-PAGE gel electrophorosis (next paragraph). When the gradient was finished, the column was washed with 100% buffer B to remove impurities and then washed with 20% ethanol before the column is stored at 4 °C.

3.2.3. SODIUM DODECYL SULFATE POLYACRYLAMIDE GEL ELECTROPHORESIS (SDS-PAGE)

Materials:

- Cell pellet and fractions from purifications (referring to paragraph 3.2.1 and 3.2.2 respectively)
- SDS-PAGE working solution
  - 5 µL NuPAGE® LDS Sample Buffer (4x)
  - 2 µL NuPAGE® Reducing Agent (10x)
  - 3 µL dH_2O.
- NuPAGE® 10 % Bis-Tris Gel 1.0 mm x 10 wells
- BenchMark™ Protein Ladder
- 1 x MES SDS Running Buffer
- Staining buffer (0.1% Coomassie R-250, 40% ethanol, 10% conc. acetate acid)
- Destaining buffer (10% ethanol, 75% concentrated acetic acid)

Method:

SDS-PAGE separates the proteins according to their sizes. According to ExPASy, CelS2 is 38 kDa and thus the purity of this protein can be examined. The SDS-PAGE was also used to determine which fractions from the purification contain this desired protein. The fractions (10 µL) were transferred to 10 µL working solution, containing 5 µL NuPAGE® Sample Buffer, 2 µL NuPAGE® Reducing Agent and 3 µL dH_2O. Then, the samples were heated up in a water bath at 70 °C for 10 min. The proteins were completely unfolded (denatured) under the heat treatment, and this reduced state was maintained due to the Reducing Agent

(dithiothreitol) that is a strong reducing agent that prevents formation of disulfide bonds (Thermo Scientific, 2017). The Sample Buffer contains **lithium dodecyl sulfate**, pH 8.4, which allows for maximum activity of the reducing agent (by binding to the hydrophobic areas of the proteins, and absence of cleavage of Asp-Pro bonds (Thermo Scientific, 2017). After the treatment, the proteins were completely unfolded and had the same shape and charge. In gel electrophoresis, the negatively charged proteins wander towards the positively pol in an electric field. The network of polyacrylamide pores in the gel makes the larger proteins wander slower compared to the small ones (Johnson et al., 2015). The Benchmark Protein Ladder (5-7.5 µL) was added to identify the band of the desired protein. The gel electrophoresis chamber was filled with 1 x MES buffer, and run on current at 200 V in 50 min.

After gel electrophoresis, the gel was added staining buffer containing Comassie Brilliant Blue that binds to proteins to visualize them in the gel. The staining reaction was accelerated by heating the gel with the staining buffer and incubating at room temperature for 5 minutes on a shaking board. The bands of proteins became visible by adding destaining buffer, heated up for one minute and incubated at room temperature for minimum 10 min on a shaking board. Those fractions that gave the strongest bonds of the desired protein in the gel, were taken to the next purification step, referring to paragraph 3.2.4.

3.2.4. CONCENTRATING PROTEIN SOLUTION WITH CENTRIFUGAL FILTERS

Materials:

- Protein solution (referring to paragraph 3.2.2)
- Amicon Ultra-15 Centrifugal Filter Unit, 10K

Method:

Centrifugal filters promote high sample recoveries, even in dilute samples, through ultrafiltration. Thus, the centrifugal filter (10 K) retains proteins larger than 10 kilo Daltons (kDa) in the filter, making it suitable for up concentration of CelS2 (38 kDa). Transfer all the protein solution to the filtrate, centrifuge at 4300 rcf, 4 °C until 1.0-1.5 mL is left in the filter. This solution will be used for the next purification.

3.2.5. SIZE EXCLUSION CHROMATOGRAPHY (SEC)

Materials:

- Up-concentrated protein solution (1.0-1.5 mL) (referring to 3.2.4)
- HiLoad™ 16/600 Superdex™ 75 prep grade
- Buffer A: Degassed 50 mM Tris-HCl pH 7.5, 200 mM NaCl
- Degassed dH_2O
- Degassed 20% ethanol

Method:

The second purification step to isolate CelS2 was done by another high performance sepharose column, the HiLoad™ 16/600 Superdex™ 75 prep grade monitored by UV detection. The column has a volume of 120 mL and operates at a flow rate of 1 mL/min. First the column was washed with 20 min of degassed dH_2O, and then equilibrated with degassed Buffer A for 120 min. The protein solution was then applied, eluted with Buffer A and collected in fractions of 2 mL (60 fractions in total). The matrix separates molecules based on their sizes. Small proteins diffuses into pores of gel beads, while larger ones have trouble to diffuse into the pores due to steric hindrance (GE Healthcare, 2017) Thus, the larger proteins elute first. The purity of CelS2 was checked on SDS-PAGE, referring to paragraph 3.3.3. After two hours of running Buffer A, the column was washed with 20 min degassed dH_2O and 2 hours with 20% ethanol before storing it at room temperature.

3.2.6. DETERMINING PROTEIN CONCENTRATION - A_{280}

Materials:

- Protein solution with isolated CelS2 (referring to paragraph 3.2.5)
- Storing buffer as a blank sample (50 mM NaH_2PO_4/Na_2HPO_4 pH 7.0)
- UVette

Method:

The protein concentration can be measured by a spectrophotometer using UV-radiation, as the aromatic amino acids phenylalanine, tyrosine and tryptophan absorbs UV and have absorption maximum at 257 nm, 274 nm and 280 nm respectively (Lesk, 2010). The concentration is determined with the Beer-Lamberts rule (Pace et al., 2015).

$$A = c\varepsilon l \quad \textbf{(3.3.1)}$$

, whereas A for absorbance, c for concentration in M, ε is the extinction coefficient and l is the length of the absorption cell. The extinction coefficient of CelS2 is calculated to be 75775$M^{-1}cm^{-1}$ by ExPASy ProtParam Tool. First, the fractions of CelS2 after SEC was up-concentrated by a centrifugal filter unit, and then the buffer was exchanged to 50 mM NaP pH 7.0 by adding 15 mL and centrifuging at 4300 rcf at 4 °C until 1.0-1.5 mL is left in the filter, four times. The concentration of isolated CelS2 was determined by adding 1 µL sample to 99 µL storing buffer. The ratio is 1/100 to measure a concentration between zero and one, as the spectrophotometer is the most accurate at this concentration range. The blank sample consists of 100 µL storing buffer.

3.3. ENZYME KINETICS

3.3.1. COPPER-SATURATING LPMO

Materials:

- Isolated CelS2 solved in 50 mM NaP pH 7.0 (referring to 3.2.5)
- 5 mM $CuSO_4$
- PD MiniTrap^{TM} G-25 column
- Storing buffer (50 mM NaH_2PO_4/Na_2HPO_4 pH 7.0)

Method:

LPMOs such as CelS2 are copper-dependent enzymes that use molecular oxygen to cleave the glycosidic bond in crystalline cellulose, previously described in section 1.2. Thus, isolated CelS2 was incubated in 30 min with 3 times the molar concentration of $CuSO_4$ compared to the enzyme concentration, to become activated. The excess of copper is removed by applying the sample to the PD MiniTrap^{TM} G-25 column. The column tolerates approximately 15.0 mg/mL $CuSO_4$, thus the concentration of isolated CelS2 should be diluted to below 5.0 mg/mL with the storing buffer. The column was equilibrated with 8 mL storing buffer before applying a 250 µL sample containing copper-saturated CelS2. The total sample volume should be 500 µL, thus 250 µL storing buffer was applied additionally with the sample. The copper-saturated CelS2 was eluded by applying 200 µL storing buffer 5 times, and collected into five fractions. The majority of CelS2 usually is collected in fraction 2. All CelS2 variants were copper-saturated prior activity assays, and their concentrations were determined in a spectrophotometer, referring to paragraph 3.2.6. Copper-saturated CelS2 usually are activated in many months, compared to CPB21 that is active in only two weeks, but they can be copper-saturated once again to keep them active.

3.3.2. LPMO ACTIVITY ASSAY

Materials:

- Copper-saturated CelS2 (wild-type and mutants) (referring to paragraph 3.3.1)
- 50 mM sodium phosphate buffer pH 7.0
- 50 g/L Avicel
- 100 mM Ascorbic acid
- 2 mL Eppendorf tubes
- Eppendorf Comfort Thermomixer with a temperature-controlled lid
- 96-well filter plate
- Vacuum manifold

Method:

Here we determine the effect of the mutations on the activity of CelS2, which gives a better understanding of the mechanism of the active site of CelS2, previously described in section 1.5. The wild-type and mutants were run on the same conditions, thus the activity of CelS2 variants are directly comparable. CelS2 is active on crystalline cellulose, thus we use Avicel as substrate for the assay. The CelS2 reactions (500 µL) contained 10 g/L Avicel and 0.5 µM isolated CelS2, buffered with 50 mM sodium phosphate buffer pH 7.0. The samples were incubated at 40 °C at 1000 rpm for 20 min on Eppendorf Comfort Thermomixer with a temperature-controlled lid. Then the samples was added a reductant, 1 mM ascorbic acid, to start the reactions. The reactions were sampled in after 20, 40, 60, 120 and 240 min, and filtrated immediately using a 96-well filter plate operated by a vacuum manifold to stop the reactions. The activity is measured by quantifying oxidized products on ICS, on the next paragraph.

3.3.3. PRODUCT ANALYSIS BY ION CHROMATOGRAPHIC SYSTEM (ICS)

Materials:

- CelS2 reactions (referring to paragraph 3.3.2)
- Dionex Bio-LC (ICS 3000) equipped with a CarboPac PA1 column
- Pulsed amperometric detector (PAD)
- Gold electrode
- Buffer A: Degassed 0.1 M NaOH
- Buffer B: Degassed 0.1 M NaOH, 1 M $NaCH_3COOH$
- Buffer C: Degassed dH_2O

Method:

Products from activity assay were separated by high performance anion exchange chromatography (HPAEC) and monitored by pulsed amperometric detection (PAD). The PAD detector takes advantage of the weakly acidic nature of carbohydrates at high pH, forces them to be electrocatalytically oxidized at the gold electrode by application of a positive potential (Rohrer, 1998; Thermo Scientific, 2017). The PAD detector measures the potential variations resulted by oxidizing and reducing conditions on the electrode surface, as the carbohydrates are oxidized when touching the working electrode surface. Pulsed amperometry detects only electroactive species, making it a sensitive and highly selective detector since many potentially interfering species cannot be oxidized or reduced, and thus are not detected. The current generated is proportional to the carbohydrate concentration, and therefore carbohydrates can be detected and quantified.

Solubilized cello-oligosaccharides from the activity assay were quantified using Dionex Bio-LC equipped with a CarboPac PA1 column operating with a flow rate of 0.25 mL/min in 0.1 M NaOH (eluent A) and a column temperature of 30 °C (Forsberg et al., 2011). Before quantification, samples were hydrolyzed with the endoglucanase Cel5A from *Thermobifida fusca* (*Tf*Cel5A), yielding oxidized products with a degree of polymerization of 2 and 3 [GlcGlc1A, $(Glc)_2Glc1A$]. Native and oxidized products were eluted and separated using an optimized stepwise gradient with increasing amount of eluent B (0.1 M NaOH, 1 M NaOAc), as follows: 0-10 % B over 10 min, 10-18 % B over 10 min, 18-30 % B over 1 min, 30-100 % B over 1 min, 100-0 % B over 0.1 min and 0 % B over 13.9 min (Westereng et al., 2013). Oxidized dimers were quantified using GlcGlc1A standards.

3.3.4. HYDROGEN PEROXIDE ASSAY

Materials:

- Copper-saturated CelS2 (wild-type and mutants) (referring to paragraph 3.3.1)
- Multiskan^{TM} FC Microplate Photometer
- Amplex® Red Hydrogen Peroxide/Peroxidase Assay Kit
- 96-well plate
- Ascorbic acid
- dH_2O

Method:

LPMOs are known to produce hydrogen peroxide (H_2O_2) when not bound to the substrate and in the presence of a reductant (Kittl et al., 2012; Isaksen et al., 2014; Loose et al., 2016; Bissaro et al., 2016). H_2O_2 produced by unbound LPMOs can be detected with the use of Amplex® Red reagent that react with H_2O_2 in a 1:1 stoichiometry and produce a red-fluorescent oxidized product, resorufin (Thermo Scientific, 2017). The reaction between H_2O_2 and Amplex® Red reagent is catalyzed by horseradish peroxidase (HRP). The H_2O_2 production of CelS2 variant was quantified by measuring absorbance at 540 nm using a Multiskan FC spectrophotometer.

The reaction sample consists of a working solution (100 µM Amplex® Red reagent, 5 U/mL HRP, and 50 mM sodium phosphate buffer, pH 7.0) mixed with 2 µM CelS2 in a total sample volume of 180 µL. Before starting the reaction, the samples were equilibrated in the spectrophotometer. The reaction started when adding 20 µL ascorbic acid (final concentration of 50 µM), and H_2O_2 production was quantified during the incubation of the sample reaction for 30 min at room temperature. Three parallels were used. The standard curve, ranging from 10 to 40 µM, was made by diluting the H_2O_2 standard stock solution supplied with the kit.

An additional round of this experiment was done but with the addition of 0.25 µM superoxide dismutate (SOD), to test two hypotheses for probing the reaction mechanism of LPMO for producing H_2O_2 (further described in section 1.2.8).

4. RESULTS

4.1. SEQUENCE ANALYSIS AND MUTANT DESIGN

Amino acids close to the copper-coordinating center were selected for mutation to gain insight in their roles regarding LPMO activity, further described in section 1.5. The chosen mutations, shown in Table 2.7, were generated using QuikChange II Site-Directed Mutagenesis Kit, referring to section 3.2. To verify that the desired mutations were incorporated and random mutation did not appeared, the mutated plasmid was sent to GATC Biotech in Konstanz, Germany, for DNA sequencing. The results from sequencing were analyzed in the software CLC DNA Workbench, which aligns the wild-type DNA sequence with the mutated one, as shown in Figure 4.1.1. The Figure shows the point mutations that we applied as ¨Conflicts¨, and as no other similar messengers were found, we concluded that the mutation was successful. Similar successes were found for the other mutations (results not shown).

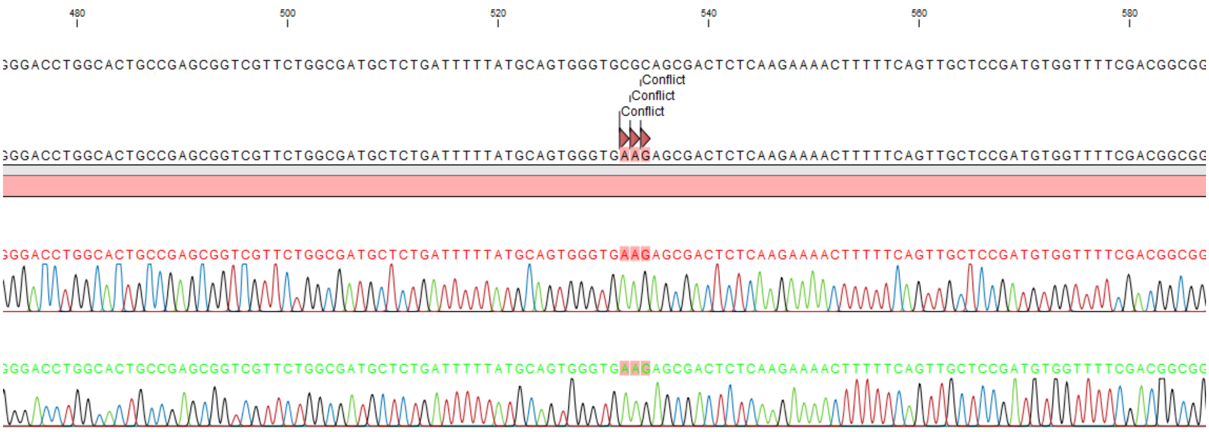

Figure 4.1.1. Sequence alignment of CelS2-WT and CelS2-R212K. The sequence at the top is the wild-type sequence, and the consensus consists of the two parallels of mutated sequences below. The nucleotides marked ¨Conflicts¨ indicates that CGC that codes for arginine in the wild-type is mutated into AAG that codes for lysine.

4.2. PURIFICATION OF CELS2

CelS2 was released and gathered by periplasmic extraction, as verified by **Figure 4.2.2** in well 2. The extract containing CelS2 was first purified on ion exchange chromatography (**Fig. 4.2.1**), as described in section 3.3. The fractions from IEC showing the strongest bands of CelS2, verified in gel electrophoresis, were further purified on size exclusion chromatography as the final step. The purity of isolated CelS2 was once again verified on gel electrophoresis, shown in **Figure 4.2.4**. The mutants were purified on the same manner as the wild-type, thus, one set of chromatograms is used in this section to represent purification of all CelS2 variants. Notably, the UV detector did not work properly and therefore we could not measure the rise of conductivity as the gradient ran, which could give insight in which salt concentration CelS2 usually elutes.

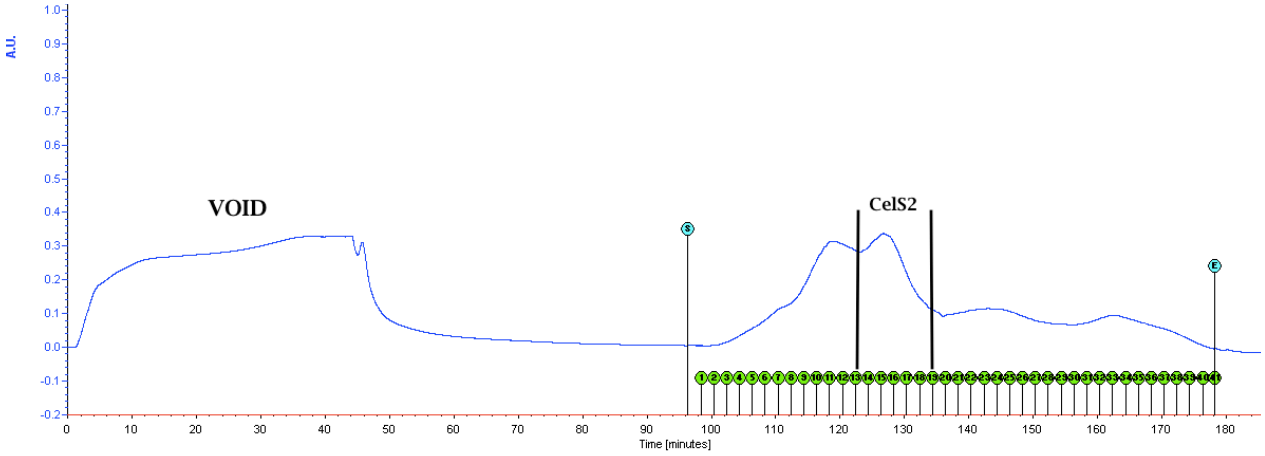

Figure 4.2.1. Chromatogram for purifying CelS2-E217N on an ion exchanger. As the periplasmic extract is applied into the column, a broad peak arises at the start of the chromatogram that contains contamination and undesired proteins. The peak, between two black bars, contains CelS2, as verified by gel electrophoresis.

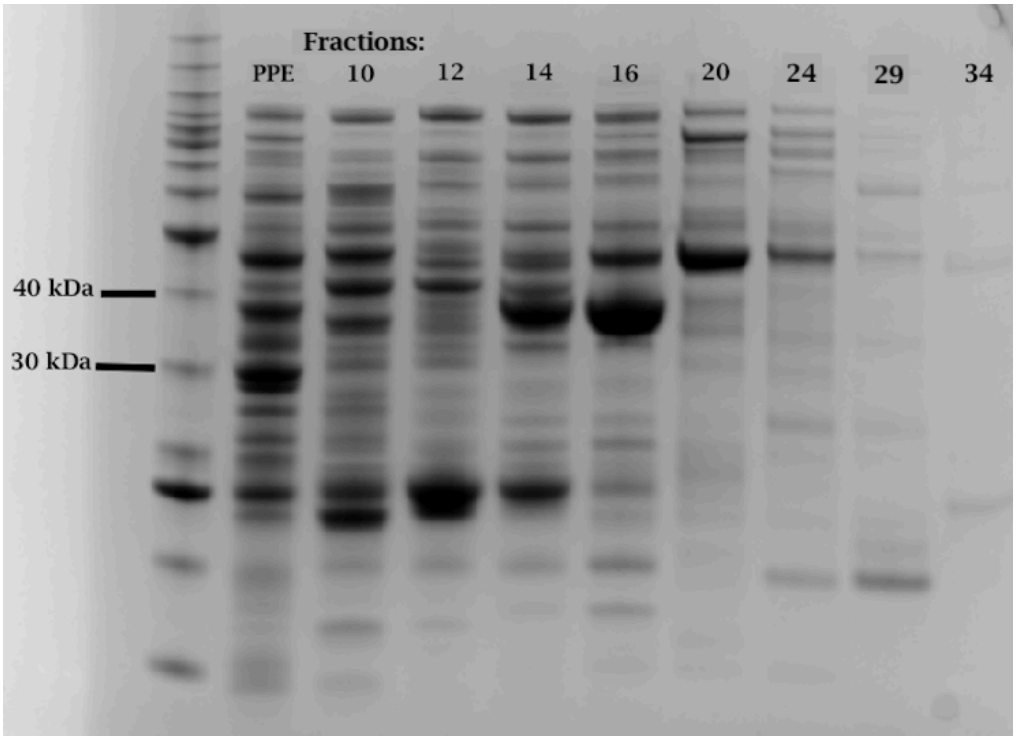

Figure 4.2.2. SDS-PAGE gel electrophoresis of the fractions containing CelS2 E217N (38 kDa) from ion exchange chromatography. Well 1 contains the Benchmark Ladder, well 2 contains the periplasmic extract containing CelS2, and well 3-10 while the other wells contains the chosen fractions from IEC purifications shown in Figure 4.2.1.

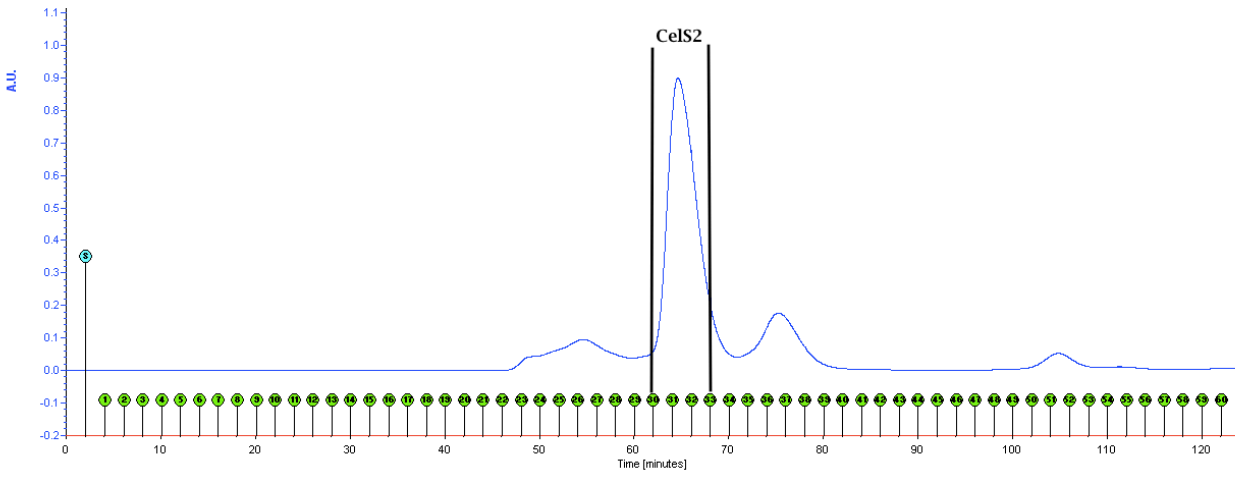

Figure 4.2.3. Chromatogram for isolating CelS2 E217N in size exclusion chromatography. The isolated CelS2 is eluted as one thin and tall peak, marked with two black bars, as verified my gel electrophoresis.

4.2.1. OVERALL RESULTS OF PURIFICATION

CelS2 variants were all purified on the same manner, with 2 purification steps after periplasmic extractions. The purity of the isolated CelS2 variants is shown in **Figure 4.2.4**. The purity of the CelS2 variants was approved. Thus, the CelS2 variants could be used for enzym activity assay.

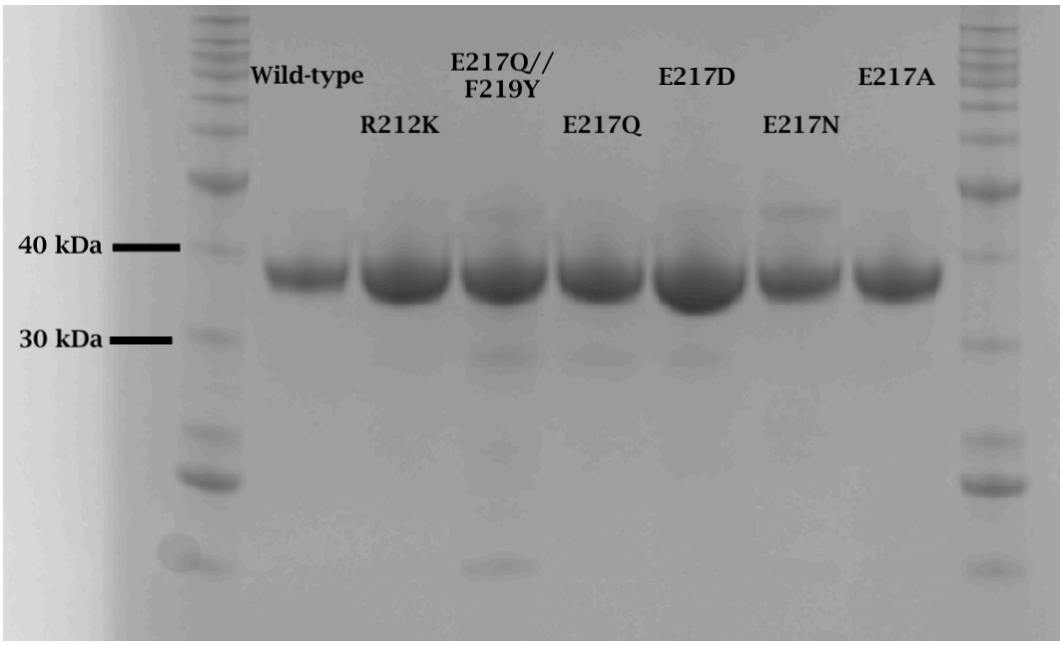

Figure 4.2.4. SDS-PAGE gel electrophoresis of isolated CelS2 variants (38 kDa). Well 1 and 9 is added Benchwork Ladder.

4.2.2. CONCENTRATION OF ISOLATED CELS2 - A_{280}

After purification and up concentration, the concentration was determined by measuring A_{280} and are shown in Table 4.2.1.

TABLE 4.2.1. Expression yield measured in mg/L from culture media for the CelS2 variants.

Enzyme	Yield	Culture media	mg/L yield
Wild-type	2.1 mg	1.0 L	2.1
R212K	17 mg	2.3 L	7.6
E217Q//F219Y	5.2 mg	2.4 L	2.2
E217Q	14 mg	4.0 L	3.5
E217D	7.2 mg	1.6 L	4.5
E217N	10 mg	2.3 L	4.4
E217A	5.6 mg	0.8 L	7.0

4.3. DETERMINING THE INITIAL RATES OF CELS2 ACTIVITY

CelS2 is thought to act on the crystalline surface of cellulose particles, therefore Avicel was used as the substrate for CelS2 activity assay. Only products with low degree of polymerization (DP) are likely to dissociate into solution (around DP8 and lower according to Brown, 2004), meaning that proper analysis of LPMO activity requires solubilization of oxidized products. The latter can be achieved by incubating the reaction mixtures with a large amount of cellulases after stopping the CelS2 reaction, as described in section 3.4.4. This procedure yields a simple mixture of oxidized products to analyze: $DP2_{ox}$ and $DP3_{ox}$. As we had only the standards of $DP2_{ox}$, only $DP2_{ox}$ products were used for find the initial activity rates for the CelS2 variants, shown in Figure 4.3.1. The Figure shows that only R212K and E217Q mutants are active, which are as active as the wild-type.

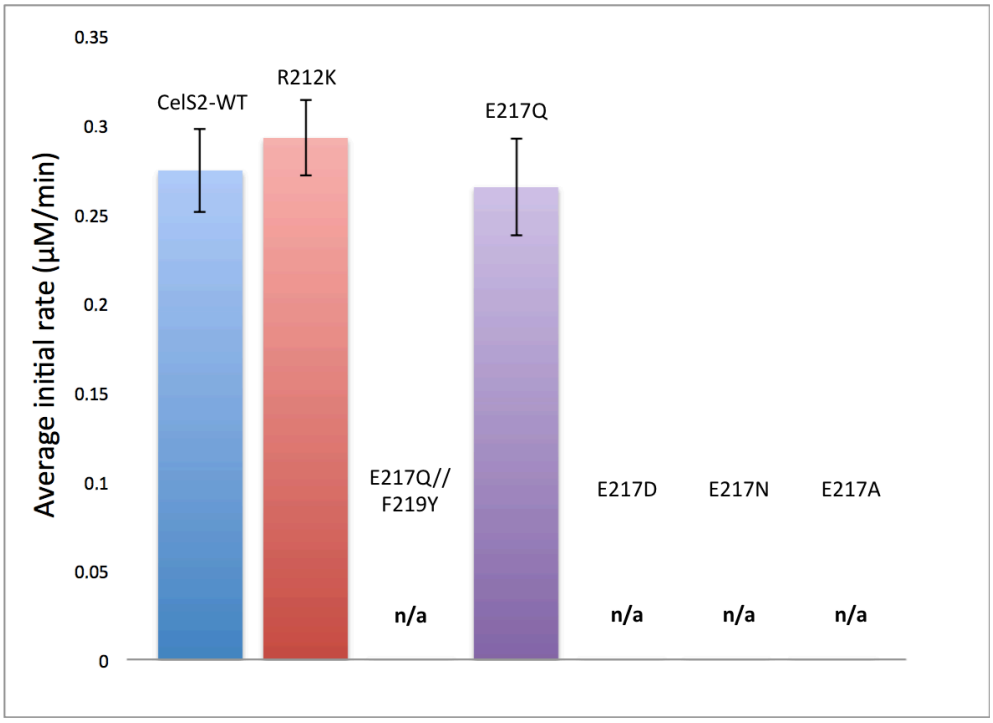

Figure 4.3.1. Activity rate comparison of CelS2 variants. Three parallels were used in the reaction assay (n=3). **n/a = no activity.**

4.4. PROBING THE H_2O_2-PRODUCING PATHWAY OF LPMO

LPMOs are well known to generate H_2O_2 when unbounded to substrate, which may aid substrate-bound LPMO to progress the catalysis (Bissaro et al., 2016; Loose et al., 2016; Isaksen et al., 2014). CelS2-WT and E217 mutants were used for activity assay with the absence of substrate, to determine the mutational effect on H_2O_2 production. Additionally, in the second round of activity assay, the samples were added superoxide dismutase (SOD) to confirm or disprove the hypothesis described in section 1.2.8. The raw data was converted into H_2O_2 concentration (µM) with the use of the extinction coefficient 0.0191 Abs/µM, and the maximum amount of H_2O_2 produced from CelS2 variants are displayed in Figure 4.4.1. The Figure suggests that only the wild-type and E217Q are active H_2O_2 producers, and they were therefore used further for comparison the average initial rate in the presence of SOD or not, shown in Figure 4.4.2.

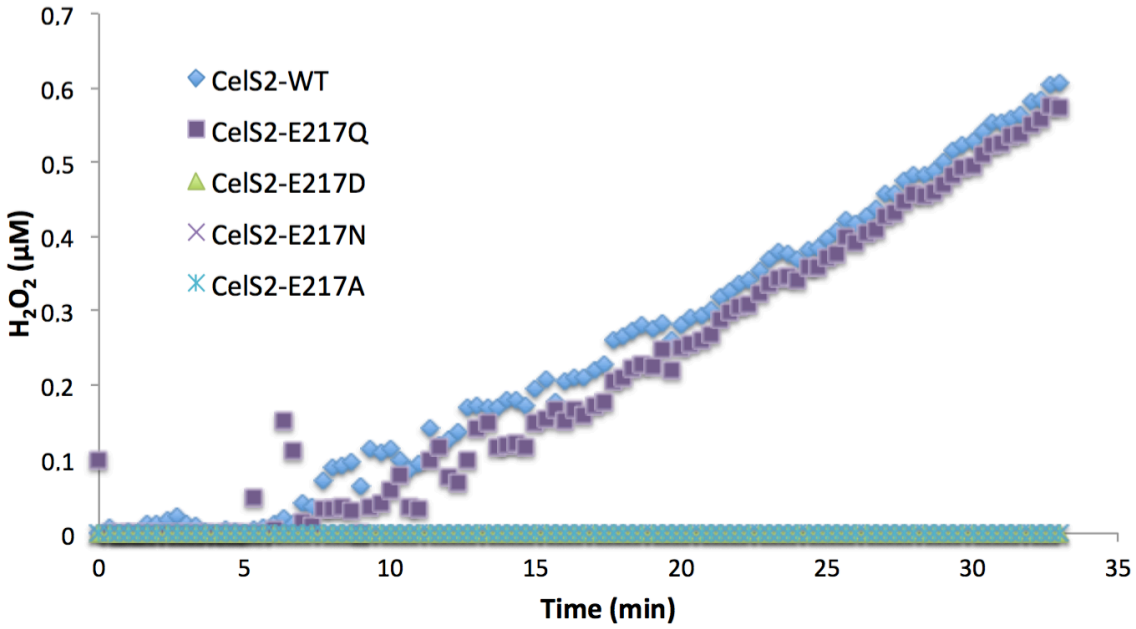

Figure 4.4.1. H_2O_2 production of CelS2 variants. n=3.

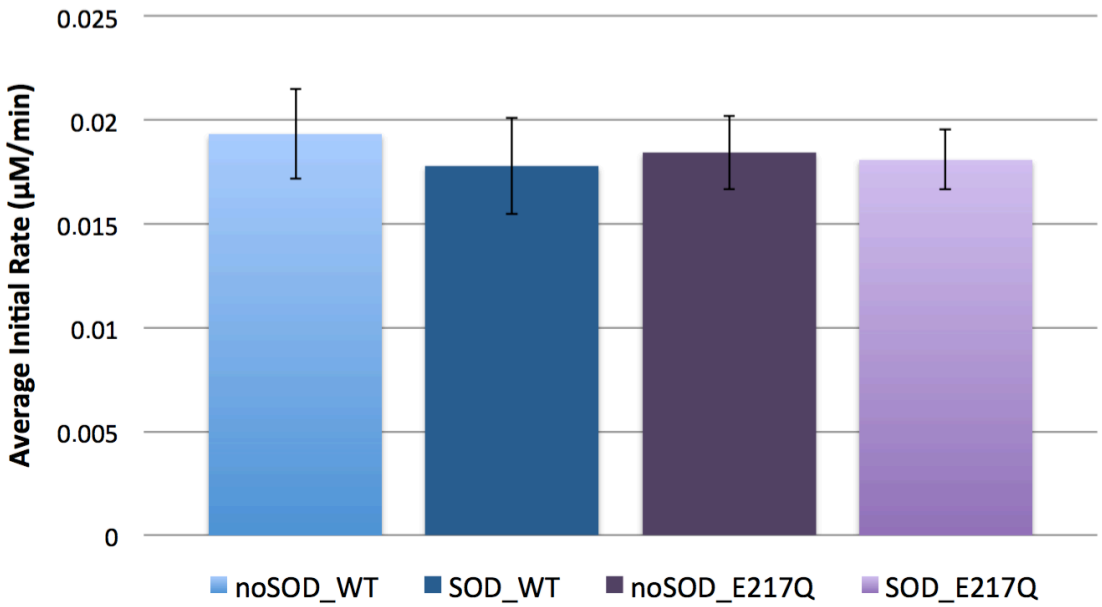

Figure 4.4.2. Activity rate comparison between CelS2-WT and CelS2-E217Q in the production of H_2O_2. The reaction samples that were not added SOD, are marked as ¨noSOD¨ under the bars. H_2O_2 production of CelS2 variants in the presence of SOD, are marked ¨SOD¨ under the bars. n=3.

5. DISCUSSION

5.1. DISCUSSING MUTATIONAL EFFECT ON CELS2 DURING CATALYSIS

The essential improvement done by LPMOs in polysaccharide degradation, have placed these enzymes at the center of worldwide research conducted on biomass conversion. Despite the great interest in their ability to cleave crystalline cellulose and chitin, little is done to probe the roles of individual amino acids involved in catalysis. With the use of several site-directed mutagenesis, this thesis will provide some insight in the function of two charged amino acids in the active site of CelS2, glutamate (E217) and arginine (R212). Site-directed mutagenesis data is scarce, making the interpretation of the their function complicated. Especially probing how residues affect each other in whole, and how the applied mutation may disrupt the synergy. Thus, more fundamental data is needed to understand the whole ¨picture¨ of the interaction between amino acids near the active site of LPMOs. Our mutagenesis data provides an understanding of the charged amino acids in close proximity to the copper ion, which will provide a basis for further studies to unveil the molecular basis of LPMO activity.

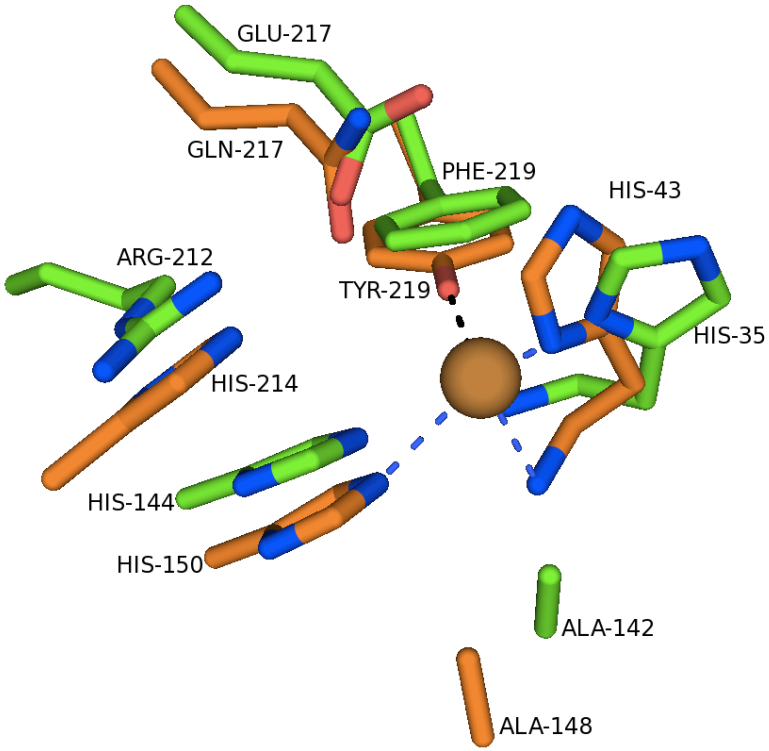

Figure 5.1.1. Comparison of two distinct active site architectures. Depicting CelS2 (PDB id: 4OY7) with green amino acids and *Sc*LPMO10B (PDB id: 4OY6) as orange. CelS2 have the conserved motif R-X_4-E-X-F while *Sc*LPMO10B have H-X_2-Q-X-Y. The active site architecture to *Sc*LPMO10B resembles those found in the cellulose-active AA9 enzymes. The copper ion is shown as a dull-orange colored sphere.

MUTANT VARIANTS OF E217

According to several LPMO structures that are characterized so far, one may make the generalization that only cellulose-active LPMOs have glutamine (Gln217; *Sc*LPMO10B numbering) in close proximity to the copper ion (**Fig. 5.1.1**), while chitin-active LPMOs have glutamate in this position (for example Glu217 in CelS2 and Glu60 in CBP21). Then, comes the exception with CelS2, that have glutamate (Glu217) and is able to perform oxidation on cellulose. Additionally, several LPMO structures show that glutamate and glutamine interact with the equatorial-positioned water molecule (**Fig. 5.1.2**, notice Glu60) towards copper ion, whereas CelS2 show similar water clusters in the active site. During catalysis, the water molecule is most likely replaces by co-substrates such as H_2O_2 and O_2. Thus, several site-directed mutagenesis were conducted in this thesis to examine the function of glutamate (E217) in CelS2.

To examine the function of CelS2-E217, the glutamate was mutated into glutamine (E217Q), aspartate (E217D), asparagine (E217N) and alanine (E217A). Aspartate has a shorter carbon chain (one -CH2- less) than glutamate which positions the carboxylate group further away from the copper ion. The results, shown in Figure 4.3.1, show that mutant CelS2-E217D has no activity at all, indicating that glutamate is essential for catalysis. Additionally, glutamate was mutated into alanine (E217A) to remove the carboxylate group, which also proves to be detrimental for activity. These results are in consensus with previous study to Harris et al. (2010) and Loose et al. (2016b) with their respective mutants Q151L in *Tt*LPMO9 and E60A in CBP21, which showed no activity either. A final test was conducted with mutant E217Q to determine if glutamate and glutamine may have the same function, and according to our results the E217Q mutant was as active as the wild-type. Altogether indicate that glutamate and glutamine are important in catalysis, as CelS2-E217, *Tt*LPMO9-Q151 and CBP21-E60 cannot function in the absence of glutamate or glutamine in this position. Thus, we propose that glutamate (E217) and glutamine (Q217, *Sc*LPMO10B numbering) coordinate the co-substrate towards the copper ion for the formation of superoxide (O_2^{*-}), catalyzing the oxidative cleavage on cellulose and chitin.

The negative charge of glutamate was also examined to test if Glu217 can act as an acid or base during catalysis. For this purpose, E217Q and E217N mutants were made to remove the charge. As E217D did not function, E217N did not function either. In previous paragraph, we determined that CelS2-E217Q functioned as efficiently as the wild-type, thus indicating that glutamate is most likely not involved in catalysis as an acid or a base. This is in consensus with glutamine in cellulose-active LPMOs as the residue is not ionizable. Thus, indicating once again that glutamate (E217 in CelS2) and glutamine (Q217 in *Sc*LPMO10) may have the same function in catalysis.

The presence of charges in the active site may be tolerated in different degree for individual LPMOs. CBP21 with a negatively-charge glutamate and no-paired positively charged amino acids, display a local negative charge near the copper ion, while the E217Q mutant in CelS2 display a local positive charge. In an independent study of Harris et al (2010), made the mutant Q151E that almost abolished the activity of *Tf*AA9. Cellulose-active LPMO (excluding CelS2) displays a neutral pair with glutamine and adjacent histidine (H214; *Sc*LPMO10B numbering), whereas the charge neutrality may be required for their activity. The charge neutrality with the pair Glu217 and Arg212 in CelS2 was eliminated by E217Q, but this mutation did not affect its activity negatively. How the negative charge affect the active site of *Tf*LPMO9 is currently unknown. Chitin-active LPMOs and CelS2 may tolerate the local charge better than other LPMOs. Thus, the effect of exchanging glutamate and glutamine should be studied further with several other LPMOs. X-Ray crystallography may shed some light into this matter. Either way, we know for certain that CelS2 function as efficient with glutamine (E217Q) as with glutamate (E217).

R212K

Cellulose-active LPMOs, in contrast to CelS2, have an additional histidine residue (H214) that lie in close proximity to the second histidine in the histidine brace (H150) (*Sc*LPMO10B numbering) (**Fig. 5.1.1**). The alignment of the aromatic rings of these two histidine residues indicates a hydrophobic stacking interaction, which may provide stability to the histidine brace during catalysis. Arginine (R212) in CelS2 is in the corresponding position as H214 in *Sc*LPMO10B. Furthermore, the guanidinium group in arginine has a planar geometry with three amino groups that resemble the imidazole ring to histidine in some degree. Thus, arginine may provide the same stabilizing effect as H214 to the histidine brace. In this thesis, we eliminate the guanidinium group by mutating arginine into lysine (R212K), which is a flexible carbon chain with one amino group. According to our results (**Fig. 4.3.1**), the R212K mutant was as active as the wild-type, and thus, the guanidinium and amino group made no difference to the activity of CelS2. One should examine if the second histidine in the histidine brace need further stabilization, as chitin-active LPMOs such as CBP21 display a cavity in this position. The cavity seen in most chitin-active LPMOs has been suggested to accommodate O_2 (Hemsworth et al., 2013b) or the N acetyl moiety of chitin chain (Forsberg et al., 2014a). Recently, Loose et al. (2016b) performed site-directed mutagenesis on isoleucine (I180) in CBP21 into arginine to fill the cavity and also to resemble the chitin-active *Cj*LPMO10. The mutant I180R almost completely abolished catalysis, which is likely due to the introduction of a positive charge that may be positioned too close to the copper ion. X-Ray crystallography may shed some light into this matter. Therefore, more fundamental data is needed to understand the role of Arg212 in CelS2, His214 in *Sc*LPMO10B and the cavity to CBP21.

Another possible function to arginine in CelS2 is to coordinate glutamate (Glu217) towards the copper ion. It is well known that arginine frequently forms salt-bridges with negatively charged amino acids nearby. In other cellulose-active LPMOs, glutamine is paired with the additional histidine (H214, *Sc*LPMO10B) most likely through hydrogen bonds. Additionally, tyrosine (Y219) interact with glutamine (Q217) in cellulose-active LPMOs (*Sc*LPMO10B), as pointed out by Harris et al. (2010) and Beeson et al. (2015). Previously, we have observed that the positioning of the carboxylate group is important (according to E217D). Both arginine and H214 may contribute to stabilize the positioning of the polar group to glutamate or glutamine. In chitin-active LPMOs that have the cavity next to the active site, display an asparagine (N185; CBP21 numbering) that points the polar group outward from the copper

ion (**Fig. 5.1.2**). This asparagine residue is close enough to interact with glutamate likely through hydrogen bonds. Recently, Loose et al. (2016b) mutated asparagine (N185) in CBP21 into alanine, and the mutation reduced CBP21 activity to around 25% activity. Thus, indicating that asparagine (N185) in CBP21 is not important for catalysis (as the activity was not abolished) but may be important for stabilizing glutamate (E60) of contribute to water clustering near the active site.

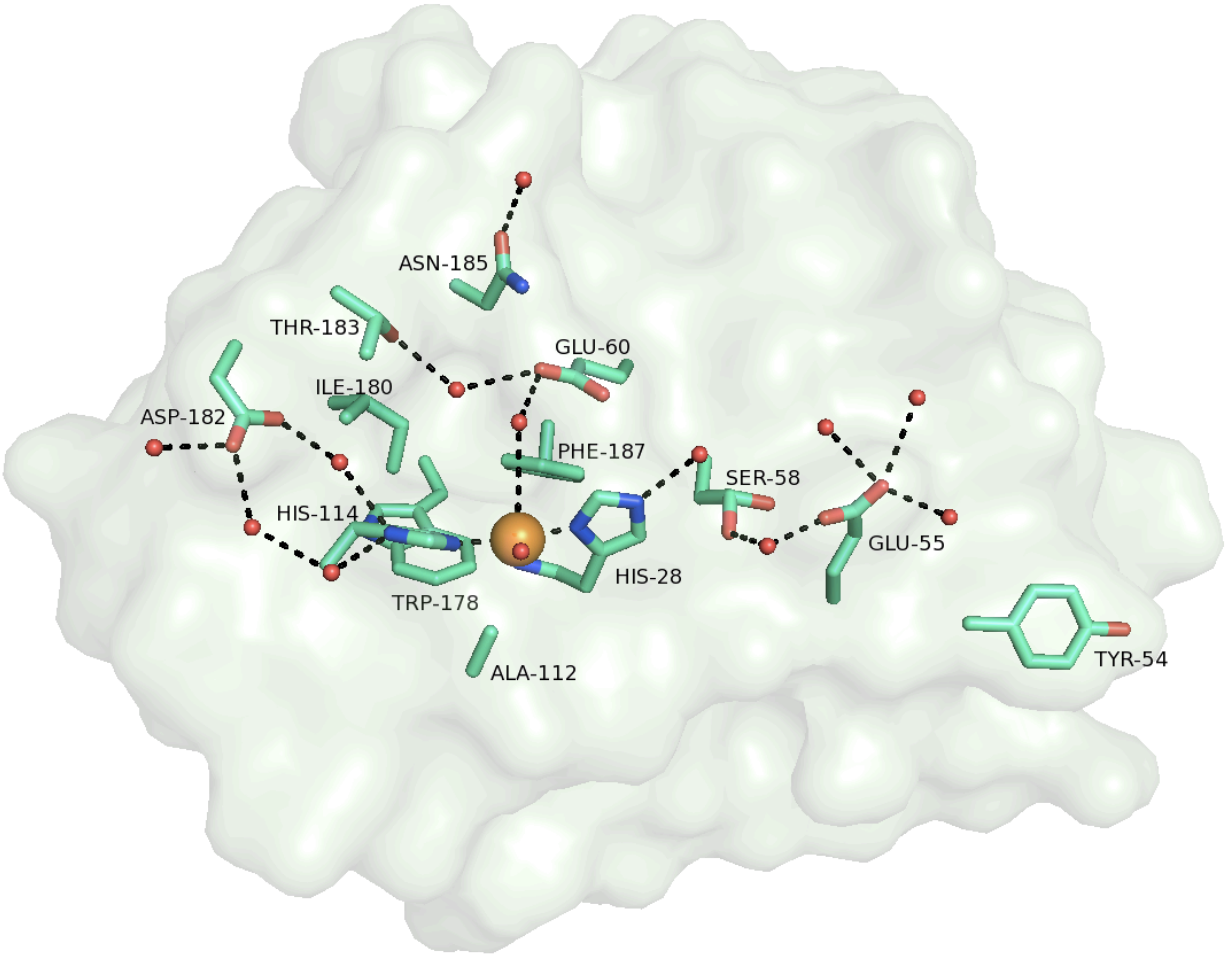

Figure 5.1.2. Essential residues for CBP21 activity and the water clustering around the active site. These residues were shown to be important for CBP21 activity either for binding to substrate of catalytic properties, by the several site-directed mutagenesis conducted by Loose et al (2016b). The copper ion is shown as an orange sphere, and the water molecules as small red spheres.

E217Q//F219Y

This mutation was part of an early experiment with ScLPMO10B in this thesis. The main purpose of the double mutant E217Q//F219Y in CelS2 was to mimic the active site of *Sc*LPMO10B (Q217 and Y219), and vice versa with *Sc*LPMO10B with the double mutant Q217E//Y219F. However, *Sc*LPMO10B proved to be difficult to work with, as we could not manage to make mutants with *Sc*LPMO10B. Fortunately, the double mutant with CelS2 was made.

The first hypothesis was that glutamate and glutamine found in CelS2 and *Sc*LPMO10B function in the same way, but this was proved without *Sc*LPMO10B. The second hypothesis is that tyrosine and phenylalanine have the same function. Phenylalanine likely restricts binding to ligand in this position with steric hindrance, while tyrosine act as the axial-copper ligand with its hydroxyl group. The clear difference between these is that tyrosine contribute to form an octahedral geometry, while phenylalanine together with alanine (A142; CelS2 numbering) form a compressed trigonal bipyramidal geometry. These geometries may indicate different properties that contribute to catalysis. According to the proposed reaction mechanism by Marletta's research group (Beeson et al., 2015; Phillips et al., 2011), they have postulated that tyrosine might stabilize the formation of the copper ion and superoxide during catalysis. According to our results (**Fig 4.3.1**), the double mutant of CelS2 showed no activity. This is in consensus with what Forsberg et al. (2014b) observed with the single mutant F219Y in CelS2, as already with the single mutant proved to be detrimental to the CelS2 activity. Later Forsberg et al. (2014b) used X-Ray crystallography on CelS2-F219Y and discovered that the hydroxyl group added on the Cζ of the phenylalanine side chain is positioned too close to the copper ion (resulting 1.7Å according to **Fig. 5.1.3**). In other cellulose-active LPMOs, the distance between the hydroxyl group of tyrosine and the copper ion is around 2.8 Å (Beeson et al., 2015), whereas the aromatic ring are positioned further away from the copper site to avoid steric hindrance and form the octahedral geometry. Interesting, CelS2-F219Y showed a similar Electron Paramagnetic Resonance (EPR) spectra as the wild-type, indicating that the copper ion is still bound to the histidine brace. Though the copper ion in this state cannot perform oxidative cleavages.

In an independent study, Harris et al. (2010) mutated tyrosine (Y153) in *Tt*LPMO9 into a phenylalanine, and their results showed that the activity was reduced substantially but not fully eliminated. We postulates that the C ζ of the phenylalanine side chain (Y153F) may be positioned to far from the copper ion to fully function as steric hindrance for ligand binding axial to the copper ion. Additionally, Forsberg et al. (2014b) mutated phenylalanine in CelS2 (F219) into alanine, and surprisingly, showed a reduced but not abolished activity. Thus, F219A indicates that the aromatic ring is not essential for LPMO activity (Forsberg et al., 2014b).

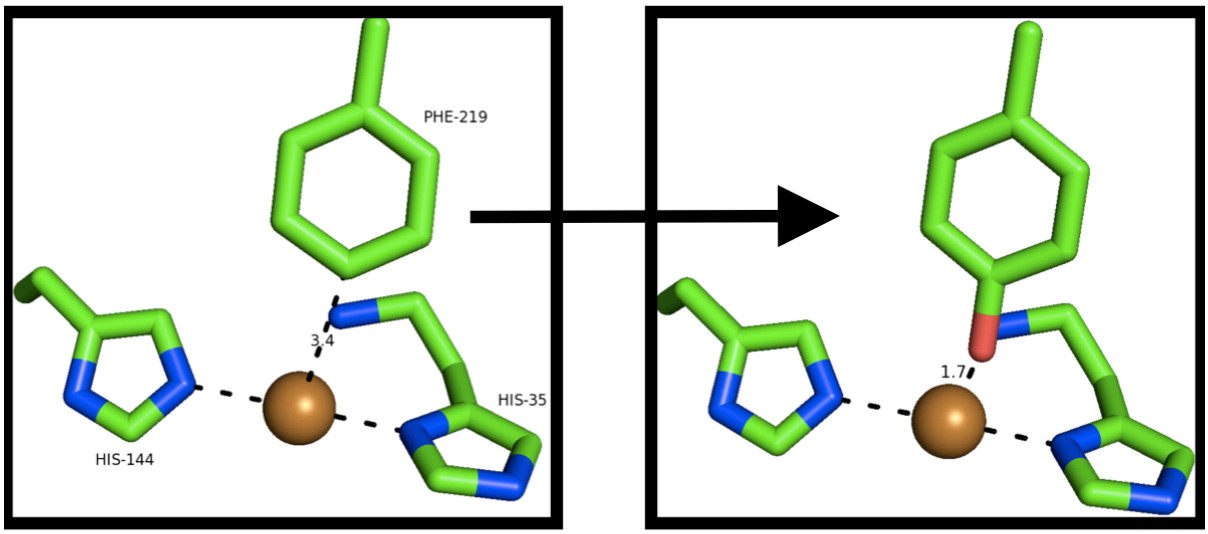

Figure 5.1.3. The mutation of phenylalanine (Phe219) in CelS2 into tyrosine. According to the wizard tools of PyMOL, the distance between the copper ion and tyrosine is 1.7 Å, which is 3.4 Å for the wild-type.

5.2. DISCUSSING H2O2-PRODUCING PROPERTIES OF CELS2 VARIANTS

According to the data, shown in Figure 4.4.1 and 4.4.2, only the wild-type and E217Q mutant produced H_2O_2, which is in consensus with the fact that only E217Q is active among E217 mutants. Furthermore, suggesting that neither E217D nor E217N could generate superoxide.

The activity assay was conducted again, but now by adding superoxide dismutase (SOD) into the CelS2 samples. The purpose was to examine how H_2O_2 is formed after the formation of superoxide in the presence of molecular oxygen and a reductant. We have two hypotheses: (i) The superoxide is released into the environment and formed into H_2O_2 through dismutation. SOD is added in the samples to catalyze the dismutation of superoxide radical (O_2^{*-}) into H_2O_2. (ii) Dismutation happens inside the active site. If the first hypothesis was true, we would most likely observe a higher concentration of H_2O_2 in the solution; and if the second hypothesis is true, the [H_2O_2] will remain the same.

Surprisingly, none of the hypotheses were confirmed, as we observed a decreased amount of H_2O_2 in the samples. Thus, the results did not make much sense. Later, the effect of SOD on H_2O_2 alone was examined further by conducting an additional assay with only the H_2O_2 standards, whereas two parallels was used where one parallel of standards was added SOD and the other was not. These two parallel had similar amount of H_2O_2, which indicate that the interaction between SOD and CelS2 may have affected the amount of H_2O_2 in the solution. The latter may be reflected by Figure 4.4.2, as the activity rate of CelS2-WT in the presence SOD is a bit lower than when SOD was not added. Finally, the overall amount of H_2O_2 produced by CelS2-WT was very low, under 1 μM H_2O_2 was produced both when SOD was/was not added. When Loose et al (2016a) conducted this assay with CBP21, they observed a H_2O_2 production to almost 60 μM after an hour. Altogether, this assay needs to be conducted again when the optimized conditions are found. It is also recommended to compare the results with the H_2O_2-producing properties of other LPMOs.

5.3 CONCLUDING REMARKS AND PERSPECTIVES

The discovery of LPMOs, capable of cleaving crystalline substrates, has changed the paradigm of enzymatic degradation of carbohydrates and thereby provided new enzyme tools for biotechnology and biorefining. Several aspect of the molecular mechanism of LPMOs, however, remains enigmatic. If LPMOs are to be optimally harnessed for industrial scale production of lignocellulosic biofuel, more fundamental work is required. The work presented in this thesis provides a basis of mutagenesis data for further studies on the molecular mechanism of LPMOs. From available functional data, it is clear that glutamate and glutamine are essential for LPMO activity.

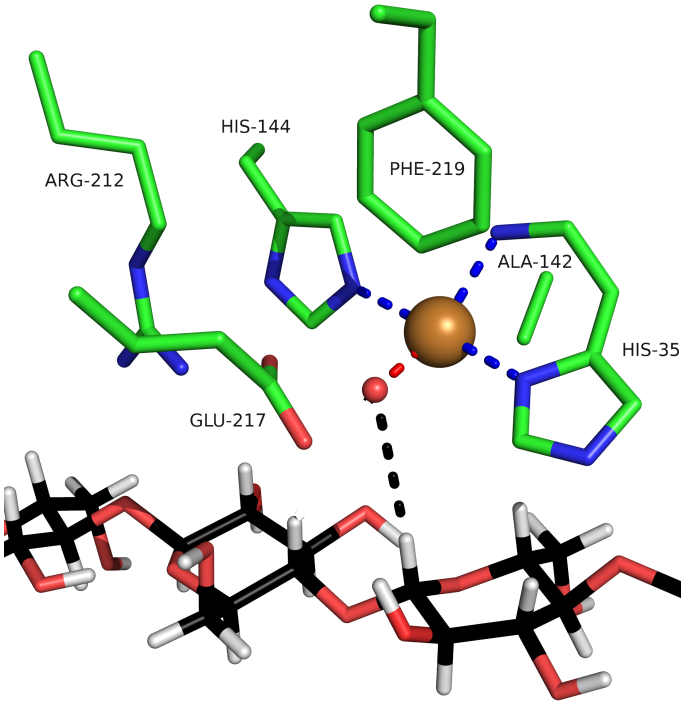

Figure 5.3.1. The active site of CelS2 (PDB id: 4OY7) catalyzing the (C1) oxidative cleavage.

6. REFERENCES

AGGER, J. W., ISAKSEN, T., VÁRNAI, A., VIDAL-MELGOSA, S., WILLATS, W. G., LUDWIG, R., HORN, S. J., EIJSINK, V. G. & WESTERENG, B. 2014. Discovery of LPMO activity on hemicelluloses shows the importance of oxidative processes in plant cell wall degradation. Proceedings of the National Academy of Sciences, 111, 6287-6292.

AGILENT TECHNOLOGIES. 2017. QuikChange II Site-Directed Mutagenesis Kit. Available from: http://www.agilent.com/cs/library/usermanuals/Public/200523.pdf

AGILENT TECHNOLOGIES. 2017. QuikChange Primer Design. Available from: http://www.genomics.agilent.com/primerDesignProgram.jsp?&_requestid=1183641

ARMESILLA, A. L., THURSTON, C. F. & YAGÜE, E. 1994. CEL1: a novel cellulose binding protein secreted by Agaricus bisporus during growth on crystalline cellulose. FEMS microbiology letters, 116, 293-299.

BECKHAM, G. T., MATTHEWS, J. F., PETERS, B., BOMBLE, Y. J., HIMMEL, M. E. & CROWLEY, M. F. 2011. Molecular-level origins of biomass recalcitrance: decrystallization free energies for four common cellulose polymorphs. The Journal of Physical Chemistry B, 115, 4118-4127.

BEESON, W. T., VU, V. V., SPAN, E. A., PHILLIPS, C. M. & MARLETTA, M. A. 2015. Cellulose degradation by polysaccharide monooxygenases. *Annual review of biochemistry,* 84**,** 923-946.

BEESON, W. T., PHILLIPS, C. M., CATE, J. H. & MARLETTA, M. A. 2011. Oxidative cleavage of cellulose by fungal copper-dependent polysaccharide monooxygenases. Journal of the American Chemical Society, 134, 890-892.

BISSARO, B., ROHR, A. K., SKAUGEN, M., FORSBERG, Z., HORN, S. J., VAAJE-KOLSTAD, G. & EIJSINK, V. 2016. Fenton-type chemistry by a copper enzyme: molecular mechanism of polysaccharide oxidative cleavage. *bioRxiv***,** 097022.

BORISOVA, A. S., ISAKSEN, T., DIMAROGONA, M., KOGNOLE, A. A., MATHIESEN, G., VÁRNAI, A., RØHR, Å. K., PAYNE, C. M., SØRLIE, M. & SANDGREN, M. 2015. Structural and functional characterization of a lytic polysaccharide monooxygenase with broad substrate specificity. *Journal of Biological Chemistry,* 290**,** 22955-22969.

CANNELLA, D., MÖLLERS, K. B., FRIGAARD, N.-U., JENSEN, P. E., BJERRUM, M. J., JOHANSEN, K. & FELBY, C. 2016. Light-driven oxidation of polysaccharides by

photosynthetic pigments and a metalloenzyme. *Nature communications,* 7.

COURTADE, G., WIMMER, R., RØHR, Å. K., PREIMS, M., FELICE, A. K., DIMAROGONA, M., VAAJE-KOLSTAD, G., SØRLIE, M., SANDGREN, M. & LUDWIG, R. 2016. Interactions of a fungal lytic polysaccharide monooxygenase with β-glucan substrates and cellobiose dehydrogenase. Proceedings of the National Academy of Sciences, 113, 5922-5927.

CROUCH, L. I., LABOUREL, A., WALTON, P. H., DAVIES, G. J. & GILBERT, H. J. 2016. The contribution of non-catalytic carbohydrate binding modules to the activity of lytic polysaccharide monooxygenases. *Journal of Biological Chemistry,* 291**,** 7439-7449.

FORSBERG, Z., MACKENZIE, A. K., SØRLIE, M., RØHR, Å. K., HELLAND, R., ARVAI, A. S., VAAJE-KOLSTAD, G. & EIJSINK, V. G. **2014a**. Structural and functional characterization of a conserved pair of bacterial cellulose-oxidizing lytic polysaccharide monooxygenases. *Proceedings of the National Academy of Sciences,* 111**,** 8446-8451.

FORSBERG, Z., RØHR, Å. K., MEKASHA, S., ANDERSSON, K. K., EIJSINK, V. G., VAAJE-KOLSTAD, G. & SØRLIE, M. **2014b**. Comparative study of two chitin-active and two cellulose-active AA10-type lytic polysaccharide monooxygenases. *Biochemistry,* 53**,** 1647-1656.

FORSBERG, Z., NELSON, C. E., DALHUS, B., MEKASHA, S., LOOSE, J. S., CROUCH, L. I., RØHR, Å. K., GARDNER, J. G., EIJSINK, V. G. & VAAJE-KOLSTAD, G. 2016. Structural and functional analysis of a lytic polysaccharide monooxygenase important for efficient utilization of chitin in Cellvibrio japonicus. Journal of Biological Chemistry, 291, 7300-7312.

FORSBERG, Z., VAAJE‐KOLSTAD, G., WESTERENG, B., BUNÆS, A. C., STENSTRØM, Y., MACKENZIE, A., SØRLIE, M., HORN, S. J. & EIJSINK, V. G. 2011. Cleavage of cellulose by a CBM33 protein. Protein Science, 20, 1479-1483.

FRANDSEN, K. E., SIMMONS, T. J., DUPREE, P., POULSEN, J.-C. N., HEMSWORTH, G. R., CIANO, L., JOHNSTON, E. M., TOVBORG, M., JOHANSEN, K. S. & VON FREIESLEBEN, P. 2016. The molecular basis of polysaccharide cleavage by lytic polysaccharide monooxygenases. *Nature chemical biology*.

FROMMHAGEN, M., SFORZA, S., WESTPHAL, A. H., VISSER, J., HINZ, S. W., KOETSIER, M. J., VAN BERKEL, W. J., GRUPPEN, H. & KABEL, M. A. 2015. Discovery of the combined oxidative cleavage of plant xylan and cellulose by a new fungal polysaccharide monooxygenase. *Biotechnology for biofuels,* 8**,** 101.

GE HEALTHCARE. 2014. Size exclusion chromatography principles and methods. Available in: http://www.gelifesciences.com/webapp/wcs/stores/servlet/catalog/en/GELifeSciences-no/service-and-support/handbooks/

GE HEALTHCARE. 2016. Ion exchange chromatography principles and methods. Available from: http://www.gelifesciences.com/webapp/wcs/stores/servlet/catalog/en/GELifeSciences-no/service-and-support/handbooks/

GUDMUNDSSON, M., KIM, S., WU, M., ISHIDA, T., MOMENI, M. H., VAAJE-KOLSTAD, G., LUNDBERG, D., ROYANT, A., STÅHLBERG, J. & EIJSINK, V. G. 2014. Structural and electronic snapshots during the transition from a Cu (II) to Cu (I) metal center of a lytic polysaccharide monooxygenase by X-ray photoreduction. *Journal of Biological Chemistry,* 289**,** 18782-18792.

HARRIS, P. V., WELNER, D., MCFARLAND, K., RE, E., NAVARRO POULSEN, J.-C., BROWN, K., SALBO, R., DING, H., VLASENKO, E., MERINO, S., XU, F., CHERRY, J., LARSEN, S. & LEGGIO, L. L. 2010. Stimulation of lignocellulosic biomass hydrolysis by proteins of glycoside hydrolase family 61: structure and function of a large, enigmatic family. *Biochemistry,* 49**,** 3305-3316.

HEMSWORTH, G. R., DÉJEAN, G., DAVIES, G. J. & BRUMER, H. 2016. Learning from microbial strategies for polysaccharide degradation. *Biochemical Society Transactions,* 44**,** 94-108.

HEMSWORTH, G. R., HENRISSAT, B., DAVIES, G. J. & WALTON, P. H. 2014. Discovery and characterization of a new family of lytic polysaccharide monooxygenases. *Nature chemical biology,* 10**,** 122-126.

HEMSWORTH, G. R., DAVIES, G. J. & WALTON, P. H. **2013a**. Recent insights into copper-containing lytic polysaccharide mono-oxygenases. *Current opinion in structural biology,* 23**,** 660-668.

HEMSWORTH, G. R., TAYLOR, E. J., KIM, R. Q., GREGORY, R. C., LEWIS, S. J., TURKENBURG, J. P., PARKIN, A., DAVIES, G. J. & WALTON, P. H. **2013b.** The copper active site of CBM33 polysaccharide oxygenases. *Journal of the American Chemical Society,* 135**,** 6069-6077.

HENRISSAT, B. 1991. A classification of glycosyl hydrolases based on amino acid sequence similarities. Biochemical Journal, 280, 309-316.

HENRISSAT, B., DRIGUEZ, H., VIET, C. & SCHULEIN, M. (1985) Synergism of Cellulases from Trichoderma reesei in the Degradation of Cellulose. Bio-Technol, 3, 722-726.

HIMMEL, M. E., DING, S.-Y., JOHNSON, D. K., ADNEY, W. S., NIMLOS, M. R., BRADY, J. W. & FOUST, T. D. 2007. Biomass recalcitrance: engineering plants and enzymes for biofuels production. *science,* 315**,** 804-807.

HORN, S. J., VAAJE-KOLSTAD, G., WESTERENG, B. & EIJSINK, V. 2012. Novel enzymes for the degradation of cellulose. Biotechnology for biofuels, 5, 1.

IGARASHI, K., WADA, M. & SAMEJIMA, M. 2007. Activation of crystalline cellulose to cellulose IIII results in efficient hydrolysis by cellobiohydrolase. Febs Journal, 274, 1785-1792.

ISAKSEN, T., WESTERENG, B., AACHMANN, F. L., AGGER, J. W., KRACHER, D., KITTL, R., LUDWIG, R., HALTRICH, D., EIJSINK, V. G. & HORN, S. J. 2014. A C4-oxidizing lytic polysaccharide monooxygenase cleaving both cellulose and cello-oligosaccharides. *Journal of Biological Chemistry,* 289**,** 2632-2642.

JOHNSON, A. B., LEWIS, J., MORGAN, D., RAFF, R. M., WALTER, P. 2015. Molecular Biology of the Cell. 6th ed. New York Garland Science.

KARKEHABADI, S., HANSSON, H., KIM, S., PIENS, K., MITCHINSON, C. & SANDGREN, M. 2008. The first structure of a glycoside hydrolase family 61 member, Cel61B from Hypocrea jecorina, at 1.6 Å resolution. *Journal of molecular biology,* 383**,** 144-154.

KITTL, R., KRACHER, D., BURGSTALLER, D., HALTRICH, D. & LUDWIG, R. 2012. Production of four Neurospora crassa lytic polysaccharide monooxygenases in Pichia pastoris monitored by a fluorimetric assay. Biotechnology for biofuels, 5, 79.

KJAERGAARD, C. H., QAYYUM, M. F., WONG, S. D., XU, F., HEMSWORTH, G. R., WALTON, D. J., YOUNG, N. A., DAVIES, G. J., WALTON, P. H. & JOHANSEN, K. S. 2014. Spectroscopic and computational insight into the activation of O2 by the mononuclear Cu center in polysaccharide monooxygenases. *Proceedings of the National Academy of Sciences,* 111**,** 8797-8802.

KURAŠIN, M. & VÄLJAMÄE, P. 2011. Processivity of cellobiohydrolases is limited by the substrate. Journal of Biological Chemistry, 286, 169-177.

LEGGIO, L. L., SIMMONS, T. J., POULSEN, J.-C. N., FRANDSEN, K. E., HEMSWORTH, G. R., STRINGER, M. A., VON FREIESLEBEN, P., TOVBORG, M., JOHANSEN, K. S. & DE MARIA, L. 2015. Structure and boosting activity of a starch-degrading lytic polysaccharide monooxygenase. *Nature communications,* 6.

LESK, A. M. (2010). Introduction to protein science : architecture, function, and genomics. 2nd ed. Oxford: Oxford University Press.

LEVASSEUR, A., DRULA, E., LOMBARD, V., COUTINHO, P. M. & HENRISSAT, B. 2013.

Expansion of the enzymatic repertoire of the CAZy database to integrate auxiliary redox enzymes. *Biotechnology for biofuels,* 6**,** 1.

LI, X., BEESON, W. T., PHILLIPS, C. M., MARLETTA, M. A. & CATE, J. H. 2012. Structural basis for substrate targeting and catalysis by fungal polysaccharide monooxygenases. *Structure,* 20**,** 1051-1061.

LIFE TECHNOLOGIES. 2010. BL21 Star™ (DE3) One Shot® BL21 Star™ (DE3)pLysS One Shot® Chemically Competent Cells. Available from: https://tools.thermofisher.com/content/sfs/manuals/oneshotbl21star_man.pdf

LOOSE, J. S., FORSBERG, Z., KRACHER, D., SCHEIBLBRANDNER, S., LUDWIG, R., EIJSINK, V. G. & VAAJE‐KOLSTAD, G. **2016a**. Activation of bacterial lytic polysaccharide monooxygenases with cellobiose dehydrogenase. Protein Science, 25, 2175-2186.

LOOSE, J. S., RØHR, Å. K., BISSARO, B., KRACHER, D., LUDWIG, R., SØRLIE, M., EIJSINK, V. G., VAAJE-KOLSTA, G. (**2016b**) Insights into catalysis by lytic polysaccharide monooxygenases through site-directed mutagenesis of CBP21 from Serratia marcescens. *Manuscript in preparation.*

MATHEWS, C. K., VAN HOLDE, K. E., APPLING, D. R., ANTHONY-CAHILL, S. J. 2013. *Biochemistry*. 4th ed. Toronto, Ont: Pearson.

MERCK MILLIPORE. 2017. Pellet Paint® Co-Precipitant. Catalogue number: 69049 Available from:https://www.merckmillipore.com/NO/en/product/Pellet-Paint-Co-Precipitant,EMD_BIO-69049-3?bd=1

NISHIYAMA, Y. 2009. Structure and properties of the cellulose microfibril. Journal of Wood Science, 55, 241-249.

OMEGA BIO-TEK. 2017. Cross Reference Guide. Available from: http://omegabiotek.com/store/product/solution-3/

OMEGA BIO-TEK. 2017. Formulas for Qiagen Kit Buffers. Available from: http://www.openwetware.org/wiki/Qiagen_Buffers

OMEGA BIO-TEK. 2013. E.Z.N.A.® Plasmid Mini Kit I, V(capped) Spin. Available from: http://omegabiotek.com/store/wp-content/uploads/2013/04/D6942.D6943.D6945-May-2013.pdf

PACE, C. N., VAJDOS, F., FEE, L., GRIMSLEY, G., GRAY, T. 1995. How to measure and predict the molar absorption coefficient of a protein. *Protein Sci.,* 4 (11): 2411-2423.

PAYNE, C. M., KNOTT, B. C., MAYES, H. B., HANSSON, H., HIMMEL, M. E., SANDGREN,

M., STÅHLBERG, J. & BECKHAM, G. T. 2015. Fungal cellulases. *Chemical reviews,* 115**,** 1308-1448.

PHILLIPS, C. M., BEESON IV, W. T., CATE, J. H. & MARLETTA, M. A. 2011. Cellobiose dehydrogenase and a copper-dependent polysaccharide monooxygenase potentiate cellulose degradation by Neurospora crassa. *ACS chemical biology,* 6**,** 1399-1406.

POMA, A. B., CHWASTYK, M. & CIEPLAK, M. 2016. Coarse-grained model of the native cellulose\ hbox {I}\ alpha and the transformation pathways to the\ hbox {I}\ beta allomorph. Cellulose, 23, 1573-1591.

QUINLAN, R. J., SWEENEY, M. D., LEGGIO, L. L., OTTEN, H., POULSEN, J.-C. N., JOHANSEN, K. S., KROGH, K. B., JØRGENSEN, C. I., TOVBORG, M. & ANTHONSEN, A. 2011. Insights into the oxidative degradation of cellulose by a copper metalloenzyme that exploits biomass components. *Proceedings of the National Academy of Sciences,* 108**,** 15079-15084.

RAGUZ, S., YAGUEA, E., WOOD, D. & THURSTON, C. 1992. Isolation and characterization of a cellulose-growth-specific gene from Agaricus bisporus. Gene, 119, 183-190.

ROHRER, J. Optimal Settings for Pulsed Amperometric Detection of Carbohydrates Using the Dionex ED40 Electrochemical Detector. Thermo Fisher Scientific Technical Note 21.1-4.

RYE, C. S. & WITHERS, S. G. 2000. Glycosidase mechanisms. Current opinion in chemical biology, 4, 573-580.

SCHNELLMANN, J., ZELTINS, A., BLAAK, H. & SCHREMPF, H. 1994. The novel lectin‐like protein CHB1 is encoded by a chitin‐inducible Streptomyces olivaceoviridis gene and binds specifically to crystalline α‐chitin of fungi and other organisms. Molecular microbiology, 13, 807-819.

SJÖSTRÖM, E. (1993) Wood polysaccharides: Wood chemistry, Fundamentals and Applications, Academic Press Inc., San Diago. 1-20, 51-70.

SPAN, E. A., SUESS, D. L., DELLER, M. C., BRITT, R. D. & MARLETTA, M. A. 2017. The Role of the Secondary Coordination Sphere in a Fungal Polysaccharide Monooxygenase. ACS Chemical Biology.

STICKLEN, M. B. 2008. Plant genetic engineering for biofuel production: towards affordable cellulosic ethanol. Nature Reviews Genetics, 9, 433-443.

SUZUKI, K., SUZUKI, M., TAIYOJI, M., NIKAIDOU, N. & WATANABE, T. 1998. Chitin binding protein (CBP21) in the culture supernatant of Serratia marcescens 2170. Bioscience, biotechnology, and biochemistry, 62, 128-135.

THERMO FISHER SCIENTIFIC. 2017. Invitrogen™ pRSET A, B and C - For high-level expression of recombinant proteins in *E.coli*. Cat. no. V351-20. Available from: https://tools.thermofisher.com/content/sfs/manuals/prset_man.pdf

THERMO FISHER SCIENTIFIC. 2016. Qubit Assay Kits. Catalog number: Q32853 Available from: http://omegabiotek.com/store/product/plasmid-mini-kit-1-q-spin/

THOMAS, L. H., FORSYTH, V. T., ŠTURCOVÁ, A., KENNEDY, C. J., MAY, R. P., ALTANER, C. M., APPERLEY, D. C., WESS, T. J. & JARVIS, M. C. 2013. Structure of cellulose microfibrils in primary cell walls from collenchyma. Plant physiology, 161, 465-476.

VU, V. V., BEESON, W. T., PHILLIPS, C. M., CATE, J. H. & MARLETTA, M. A. 2013. Determinants of regioselective hydroxylation in the fungal polysaccharide monooxygenases. *Journal of the American Chemical Society,* 136**,** 562-565.

VAAJE-KOLSTAD, G., FORSBERG, Z., LOOSE, J. S., BISSARO, B. & EIJSINK, V. G. 2017. Structural diversity of lytic polysaccharide monooxygenases. *Current Opinion in Structural Biology,* 44**,** 67-76.

VAAJE-KOLSTAD, G., BØHLE, L. A., GÅSEIDNES, S., DALHUS, B., BJØRÅS, M., MATHIESEN, G. & EIJSINK, V. G. 2012. Characterization of the chitinolytic machinery of Enterococcus faecalis V583 and high-resolution structure of its oxidative CBM33 enzyme. Journal of molecular biology, 416, 239-254.

VAAJE-KOLSTAD, G., WESTERENG, B., HORN, S. J., LIU, Z., ZHAI, H., SØRLIE, M. & EIJSINK, V. G. 2010. An oxidative enzyme boosting the enzymatic conversion of recalcitrant polysaccharides. *Science,* 330**,** 219-222.

VAAJE-KOLSTAD, G., HOUSTON, D. R., RIEMEN, A. H., EIJSINK, V. G. & VAN AALTEN, D. M. 2005. Crystal structure and binding properties of the Serratia marcescens chitin-binding protein CBP21. *Journal of Biological Chemistry,* 280**,** 11313-11319.

WADA, M., HEUX, L. & SUGIYAMA, J. 2004. Polymorphism of cellulose I family: reinvestigation of cellulose IVI. Biomacromolecules, 5, 1385-1391.

WALTON, P. H. & DAVIES, G. J. 2016. On the catalytic mechanisms of lytic polysaccharide monooxygenases. Current opinion in chemical biology, 31, 195-207.

WESTERENG, B., AGGER, J. W., HORN, S. J., VAAJE-KOLSTAD, G., AACHMANN, F. L., STENSTRØM, Y. H., EIJSINK, V. G. 2013. Efficient separation of oxidized

cello-oligosaccharides generated by cellulose degrading lytic polysaccharide monooxygenases. Journal of Chromatography A, 1271, 144-152.

WESTERENG, B., ARNTZEN, M. Ø., AACHMANN, F. L., VÁRNAI, A., EIJSINK, V. G. AGGER, J. W. 2016. Simultaneous analysis of C1 and C4 oxidized oligosaccharides, the products of lytic polysaccharide monooxygenases acting on cellulose. Journal of Chromatography A, 1445, 46-54.

WYMAN, C. E., DALE, B. E., ELANDER, R. T., HOLTZAPPLE, M., LADISCH, M. R. & LEE, Y. 2005. Coordinated development of leading biomass pretreatment technologies. Bioresource technology, 96, 1959-1966.

AACHMANN, F. L., SØRLIE, M., SKJÅK-BRÆK, G., EIJSINK, V. G. & VAAJE-KOLSTAD, G. 2012. NMR structure of a lytic polysaccharide monooxygenase provides insight into copper binding, protein dynamics, and substrate interactions. *Proceedings of the National Academy of Sciences,* 109**,** 18779-18784.

AACHMANN, F. L., VAAJE‐KOLSTAD, G., FORSBERG, Z., RØHR, Å., EIJSINK, V. G. & SØRLIE, M. 2015. Lytic Polysaccharide Monooxygenase. Encyclopedia of Inorganic and Bioinorganic Chemistry.

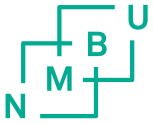

Norges miljø- og biovitenskapelig universitet
Noregs miljø- og biovitskapelege universitet
Norwegian University of Life Sciences

Postboks 5003
NO-1432 Ås
Norway